IOP Publishing Environ. Res. Lett. 20 (2025) 064039 https://doi.org/10.1088/1748-9326/adcf39

ENVIRONMENTAL RESEARCH
LETTERS

RECEIVED
16 December 2024

REVISED
24 February 2025

ACCEPTED FOR PUBLICATION
22 April 2025

PUBLISHED
23 May 2025

LETTER

Precipitation phase drives seasonal and decadal snowline changes in high mountain Asia

M Bernat[1,2,*], E S Miles[1,3], M Kneib[1,4,5], K Fujita[6], O Sasaki[6,7], T E Shaw[1,8] and F Pellicciotti[1,8]

[1] High Mountain Glaciers and Hydrology Group, Swiss Federal Institute, WSL, Birmensdorf, Switzerland
[2] LEGOS, Université de Toulouse, CNES, CNRS, IRD, UT3, Toulouse, France
[3] Glaciology and Geomorphodynamics Group, Department of Geography, University of Zurich, Zurich, Switzerland
[4] Institut des Géosciences de l'Environnement, Université Grenoble-Alpes, CNRS, IRD, Grenoble, France
[5] Department of Atmospheric and Cryospheric Sciences, University of Innsbruck, Innsbruck, Austria
[6] Graduate School of Environmental Studies, Nagoya University, Nagoya, Japan
[7] School of Environment and Society, Institute of Science Tokyo, Tokyo, Japan
[8] Institute of Science and Technology Austria (ISTA), Klosterneuburg, Austria
[*] Author to whom any correspondence should be addressed.

E-mail: maud.bernat@univ-tlse3.fr

Keywords: high mountain Asia, snow line altitude, precipitation partioning, meteorological drivers, decadal changes

Supplementary material for this article is available online

Abstract

Snow cover is of key importance for water resources in high mountain Asia (HMA) and is expected to undergo extensive changes in a warming climate. Past studies have quantified snow cover changes with satellite products of relatively low spatial resolution (∼500 m) which are hindered by the steep topography of this mountain region. We derive snowlines from Sentinel-2 and Landsat 5, 7 and 8 images, which, thanks to their higher spatial resolution, are less sensitive to the local topography. We calculate the snow line altitude (SLA) and its seasonality for all glacierized catchments of HMA and link these patterns to climate variables corrected for topographic biases. As such, the snowline changes provide a clear proxy for climatic changes. Our results highlight a strong spatial variability in mean SLA and in its seasonal changes, including across mountain chains and between the monsoon-dominated and the westerlies-dominated catchments. Over the period 1999–2019, the western regions of HMA (Pamir, Karakoram, Western Himalaya) have undergone increased snow coverage, expressed as seasonal SLA decrease, in spring and summer. This change is opposed to a widespread increase in SLA in autumn across the region, and especially the southeastern regions of HMA (Nyainqentanglha, Hengduan Shan, South–East Himalaya). Our results indicate that the diversity of seasonal snow dynamics across the region is controlled not by temperature or precipitation directly but by the timing and partitioning of solid precipitation. Decadal snowline changes (1999–2009 vs 2009–2019) seasonally precede temperature changes, suggesting that seasonal temperature changes in the Karakoram–Pamir and Eastern Nyainqentanglha regions may have responded to snow cover changes, rather than driving them.

1. Introduction

Mountain snowpacks are a key component of the water balance in the major river basins of high mountain Asia (HMA, e.g. Immerzeel *et al* 2020) and deliver seasonally-delayed discharge that is especially crucial in arid regions and drought years (Pritchard 2019). Snowpacks in the region are expected to be highly sensitive to future climate warming (Kraaijenbrink *et al* 2021) with severe consequences for vulnerable ecosystems and communities downstream (Viviroli *et al* 2020). Snow cover changes are an important control of the land surface energy balance, and can feedback to the climate system. For example, snow cover reduction is often associated with enhanced warming at high elevations through the snow-albedo feedback (e.g. Palazzi *et al* 2019), while changes in precipitation seasonality and phase can have a strong effect on mass accumulation (e.g. Jouberton *et al* 2022). A general increase in precipitation and a general decrease in snow cover are expected at the scale of HMA in the coming century, with a high spatial variability and dependence on the socio-economic pathway (Lalande *et al* 2021). Consequently, the future climate response of snowpacks is not mechanistically linked to temperature alone, although temperature changes are clearly associated with changes in snow cover seasonality (Notarnicola 2020, Tang *et al* 2022). Understanding historic snowpack dynamics and climatic controls is therefore crucial to consider the future of high-mountain catchments and of the systems that depend on their water resources.

The extremely rugged topography of HMA, combined with spatially contrasting mesoscale atmospheric drivers, leads to a diversity of climates across the region associated with a diversity of glacier mass balance patterns (e.g. Maussion *et al* 2014, Mölg *et al* 2014, Sakai and Fujita 2017). Characterizing this diversity and its evolution is hindered by the relative lack of high-elevation measurements (Tang *et al* 2013, Immerzeel *et al* 2015, Matthews *et al* 2020, Miao *et al* 2024). Therefore, researchers have favored remote sensing assessments of snow dynamics, investigating snow cover patterns (Zhou *et al* 2013, Li *et al* 2019) and trends (Smith *et al* 2017, Ackroyd *et al* 2021, Tang *et al* 2022). However, these studies have relied on coarse satellite data (e.g. MODIS at 500 m resolution) that capture the broad seasonal and spatial changes but are affected by steep topography and cloud cover (e.g. Stillinger *et al* 2019) which inhibits their reflection of fine-scale processes such as radiation-driven snowmelt (e.g. Bouamri *et al* 2021). Estimates of snow depth (Lievens *et al* 2019) and snow–water equivalent (Smith and Bookhagen 2018) rely on even coarser satellite data and/or numerical models (e.g. Liu *et al* 2021) to estimate volumes or mass at kilometer- to basin-scales. These metrics, though, due to their integration of large observational areas, are difficult to compare between domains because they also integrate dissimilar distributions of elevation, area, and aspect. Snowlines are an alternative metric of snow dynamics at the catchment and basin scale which are independent of such hypsometric biases (Krajčí *et al* 2014, Xiao and Liang 2024) while reflecting the spatial variability of the meteorology (Tang *et al* 2014). As such, they provide a clear proxy for climatic changes (McFadden *et al* 2011, Hu *et al* 2019, Aranda *et al* 2023) and are sometimes employed for quantifying and modeling interannual changes in glacier health (e.g. Klein and Isacks 1999, Rabatel *et al* 2012, Mernild *et al* 2013, Spiess *et al* 2016, Barandun *et al* 2018, Racoviteanu *et al* 2019, Tang *et al* 2020, Loibl *et al* 2025). Snowlines are most often derived from snow cover maps from optical satellite images at various spatial and temporal resolutions (Krajčí *et al* 2014, Xiao and Liang 2024). When derived from high-resolution data, they have proven useful for disentangling the meteorological drivers of seasonal snow cover change, including in catchments with steep topographies, with vertical uncertainties of the order of ~10 m (e.g. Girona-Mata *et al* 2019, Sasaki *et al* 2024). However this analysis has not previously been applied beyond individual catchments, and a comprehensive understanding of snow dynamics across HMA's varied water basins is missing.

In this study, we leverage the Google Earth Engine (GEE) archive of Landsat and Sentinel-2 high-resolution multispectral satellite images to measure snowline altitudes in all of HMA glacierized catchments, accounting for clouds, rock outcrops, glaciers, and surface water in each scene from 1999 to 2019. We use these measurements to construct a climatology of the snowline seasonal variations in each catchment across the region. We then disentangle the meteorological drivers of the variable snowline seasonality based on the ERA5-Land climate reanalysis, corrected for each catchment's hypsometric biases. Finally, we assess seasonal snowline changes between 1999–2009 and 2009–2019 and their relationship to meteorological forcings.

2. Methods

2.1. Catchment snowline altitudes

We derived snowlines for all glacierized catchments across HMA for the period 1999–2019. The catchments were defined as the intersection of the Randolph Glacier Inventory 6.0 (hereafter RGI; Pfeffer *et al* 2014) and the HydroBASINS (Lehner and Grill 2013) for the Central Asia, South Asia West, and South Asia East in RGI. We used the Pfafstetter level 9 polygons to delimit catchments of relatively similar size across the region. This resulted in 4776 glacierized catchments across the region, from 27° N to 47° N and from 66° E to 105° E (figure 1), which vary considerably in topographic distribution (SI figure 1). As all these catchments contained glaciers as of the RGI inventory date (early 2000s), we expected that they would all be affected by seasonal snow.

For each catchment we used publicly-available satellite multispectral data from 1999 to 2019 (top-of-atmosphere Sentinel-2 and Landsat 5, 7 and 8 scenes) to produce snow cover and snowline elevation time series in GEE. We filtered the scenes based on their metadata to only consider those with more than 50% cloud free area, and performed the following scene-by-scene analysis for each catchment, closely following the method developed by Girona-Mata *et al* (2019) and adapted for GEE by Sasaki *et al* (2024):

1. First, all clouds and shadows were masked within each scene to reduce false positive snow cover identification. For Landsat (30 m resolution) and Sentinel-2 (10 m resolution) sensors, we used the Quality Assessment bands which contain bitwise masks for clouds. For shadow mapping, with Landsat we adopted the approach of Miles *et al* (2017) based on the blue and near-infrared top-of-atmosphere reflectance values, using thresholds of 0.2 as in the original study. With Sentinel-2, we used the method by Hollstein *et al* (2016), tailored for this sensor. We also masked out RGI glaciers and water bodies (Pekel *et al* 2016).
2. We then identified snow-covered areas using a Normalized Difference Snow Index threshold value of 0.45 (Girona-Mata *et al* 2019). We determined the boundary of the snow-covered area and its elevation, ignoring boundary pixels adjacent to glaciers, water, clouds, and shadow (Girona-Mata *et al* 2019, Sasaki *et al* 2024).
3. We used the snow cover maps at 30 m resolution to derive monthly, seasonal and annual maps of snow cover frequency, defined as the ratio of snow observations to total observations, for each catchment for the 1999–2019, 1999–2009 and 2009–2019 study periods. We then used these results to determine the snow cover frequency distribution per elevation, based on the Advanced Land Observing Satellite (ALOS) World 3D (AW3D) 30 m digital elevation model (DEM, Tadono *et al* 2014). Monthly catchment snow line altitudes (SLA) were reconstructed using the mean elevation of the 0.5 frequency isoline of every available scene (figure 1(d)), similar to Krajčí *et al* (2014).
4. We used a second order harmonic function, a curve-fitting approach that is particularly suited to dealing with cyclical data such as seasonal changes, to fit the monthly SLAs for each catchment and each of the three study periods (Ronald Eastman *et al* 2009, Girona-Mata *et al* 2019) weighing the monthly values by the number of observations (figure 1(d)):

$$f(t) = a_0 + a_1\cos\left(2\pi\left(\Phi_1 - t\right)/T\right) + a_2\cos\left(2\times 2\pi\left(\Phi_2 - t\right)/T\right)$$

where a_0, a_1 and a_2 are the mean SLA, the first and second order SLA harmonic amplitudes, respectively. They were used to interpret the spatial and temporal variability of the SLA. Φ_1 and Φ_2 are phase parameters characterizing the timing of the SLA peaks and T the period. Such a regression can reproduce both a double and a single peak annual SLA, and the mean value and the two amplitudes, calculated directly, provide a readily accessible perspective of the spatial patterns in snowline variations across the broad region (figure 1(d)). These second order harmonic functions were used to characterize the SLA seasonality and to compare between the three study periods. The monthly temporal aggregation was applied to reduce the influence of the limited number of available satellite images, especially in the first decade (SI figures 2–4). Furthermore, given the smoothing effect from the harmonic regression, using sub-monthly data has very little effect on our results.

This method has identified snow-cover boundaries which correspond closely to manually-delineated snowlines from Landsat high-resolution multispectral imagery, while avoiding problematic deep shadows in regions characterized by steep topographies (Girona-Mata *et al* 2019). Despite differences in satellite sensors, data quality, resolution and processing between the Landsat and Sentinel-2 images, the method resulted in very close correspondence in SLA for overlapping periods at five catchments (Sasaki *et al* 2024), thus validating that the fusion of multiple data sources (from Landsat and Sentinel-2) has produced a consistent set of snowline observations.

2.2. Link with climate

Temperature, precipitation and snowfall (also referred to as solid precipitation) from ERA5-Land (Muñoz-Sabater *et al* 2021) were derived for each catchment. We consider ERA5-Land data as it has been applied to make assessments of climatological changes in HMA (e.g. Khanal *et al* 2023) or as forcing for glacier energy balance modeling (Arndt and Schneider 2023, Fugger *et al* 2024) and often is among the products with the best overall performance for those compared to ground stations (e.g. Hamm *et al* 2020, Kumar *et al* 2021, Nepal *et al* 2024), particularly for the analysis of monthly changes in temperature and precipitation. We used the minimum, maximum, mean annual, and mean June–July–August (JJA) temperature averaged over the three study periods. For precipitation and snowfall we used the mean annual, mean JJA, and mean March–April–May (MAM) values from ERA5-Land, from which we also derived solid fractions at the scale of the native grid resolution (∼9 km).

In order to remove the elevation bias of the catchments, we applied an altitudinal normalization to all climatic variables (precipitation, snowfall, and temperature) following an approach similar to that presented by Machguth *et al* (2009) and using the AW3D 30 m DEM for distributed elevation data. This approach calculates a polynomial regression of order 4 between median elevation and median climatic variable (temperature, precipitation or snowfall) of each catchment, using 40 elevation quantiles to

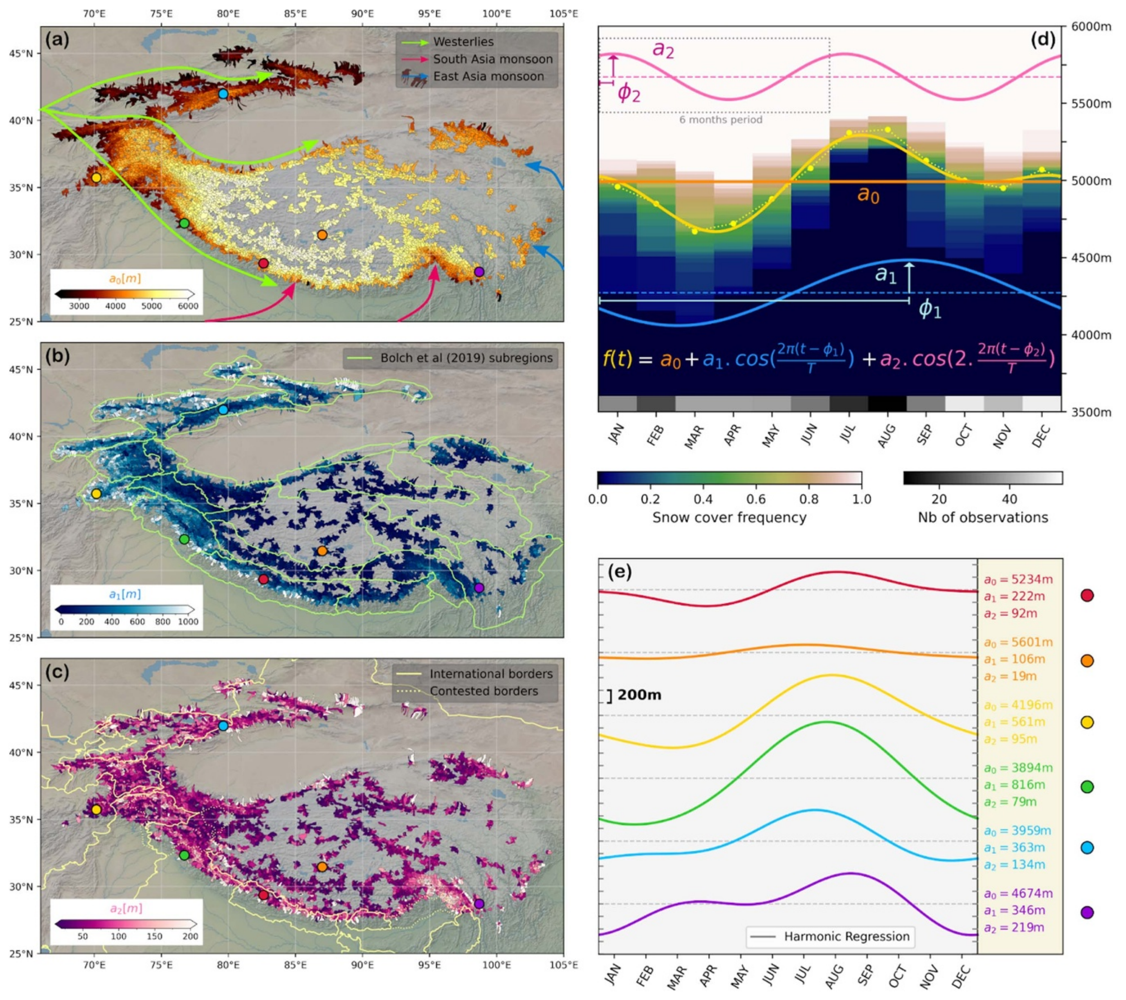

Figure 1. (a)–(c) Amplitude parameters of each catchment obtained with the second order harmonic regression. Background image was made with Natural Earth. The arrows in (a) indicate the main regional wind and precipitation patterns. (d) Example of second order harmonic regression for the period 1999–2019 for a theoretical catchment, also showing the three different terms of the harmonic function. (e) Second order harmonic regression of six catchments indicated by colored dots in maps (a)–(c). The y-axis gives the relative elevations, with the dashed lines indicating the mean elevation (a_0).

expose the underlying elevation effects (SI figure 5). The anomalies from this regression are then used to determine the catchment climatic variable values at a reference elevation of 4000 m (SI figure 5), effectively removing the elevation bias between catchments. We quantified the correlation between variables using the Spearman coefficient, using a threshold of ± 0.85 to consider the correlation significant. We used this definition to distinguish primary controls of SLA variation, which have a significant correlation with at least one amplitude parameter, from secondary controls, which have a significant correlation with at least one of the primary controls.

For the analysis of the variability in SLA in specific mountain ranges (Himalaya, Tien Shan and Kunlun-Altun Shan), we took into account the distance across each range and along each range. The distance across range was computed as the minimum length between the catchment center and the 1000 m (Himalaya)/1500 m (Tien Shan and Kunlun–Altun Shan) altitude isoline. The distance along mountains was defined as the distance from the west end of the 1000 m/1500 m altitude isoline.

3. Results and discussion

3.1. Spatial and seasonal variability of SLA across HMA

Our results show that the catchment mean annual SLA (a_0) varies considerably across the region (figure 1(a)): mean annual SLAs are highest in the interior of the Tibetan Plateau, where they can exceed 5500 m asl (figures 1(a) and (e)), and considerably lower in the north of HMA (to 3000 m asl). Mean SLAs are also relatively lower around the periphery of each major mountain belt of the region, where orographic effects may lead to enhanced snowfall at intermediate elevations (Bookhagen and Burbank 2010, Wang *et al* 2020) despite considerably higher air temperatures.

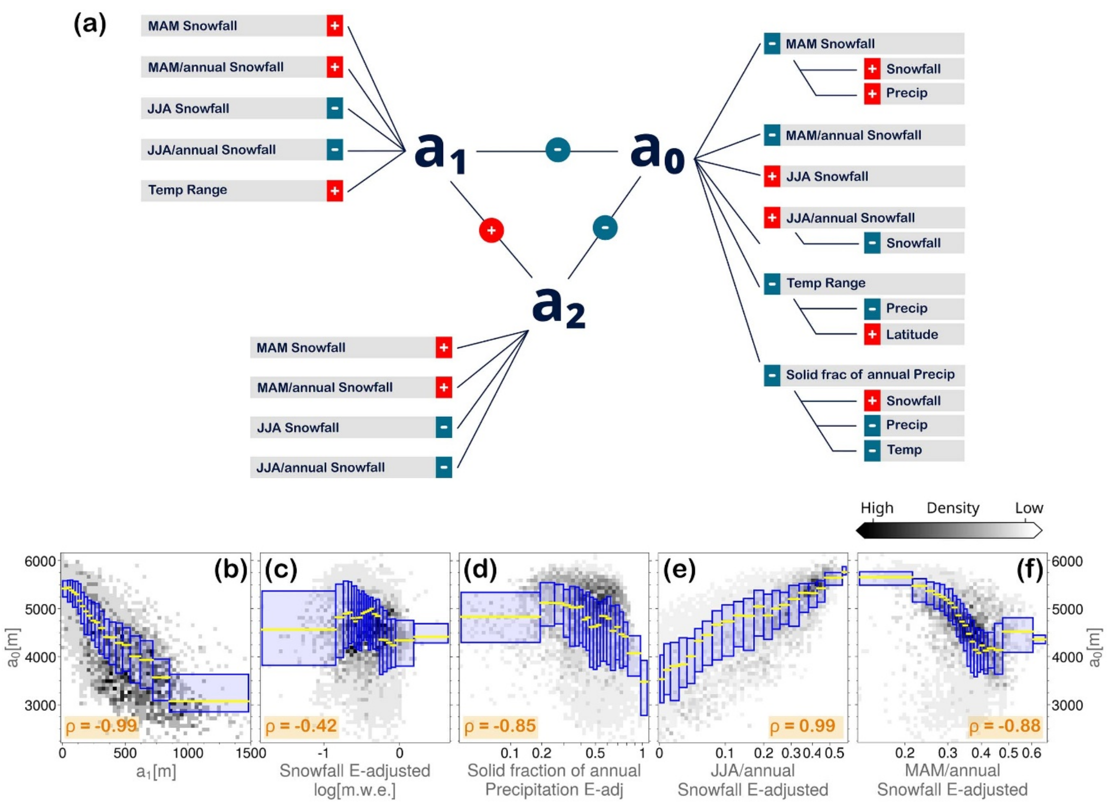

Figure 2. (a) Primary and secondary controls of the mean harmonic regression (a_0), with the sign of the Spearman's coefficient indicated in red (positive) or blue (negative). (b)–(f) Density scatter plots of a_0 as a function of a selection of primary controls. The corresponding Spearman's coefficient is indicated at the bottom of each plot. The blue boxes indicate the median and the interquartile range where each bin includes one twentieth of the data. The full correlation matrix is available in the supplementary information (SI figure 6).

The amplitude of the primary seasonal SLA harmonic (a_1) also varies continuously across the region (figure 1(b)), but is anticorrelated to a_0 ($\rho = -0.99$), demonstrating that greater SLA seasonal variability occurs for catchments with lower annual-average snowlines. The greatest seasonal amplitudes are evident for the western and southern periphery catchments (up to 1000 m), while a_1 is very low (<50 m) for catchments within the interior of the Tibetan Plateau (figure 1(e)). SLAs present much stronger seasonal patterns in Western Himalaya and Hindu Kush with annual amplitudes from 500 m to 1000 m (figure 1(e)) and a clear single peak in seasonal SLA. For other catchments, SLA variations show a secondary peak, requiring a second harmonic (a_2), for example in the Hengduan Shan ($a_2 = 200$ m to 400 m) where spring and summer both provide substantial solid precipitation (e.g. Yang et al 2013, Jouberton et al 2022, figure 1(c)). For these domains, simple onset and duration snow phenologies provide inadequate description of snow-cover variability.

Our study introduces a much greater spatial detail and accuracy than past studies of snow spatial and seasonal variability (e.g. Smith and Bookhagen 2018, Ackroyd et al 2021, Tang et al 2022) due to the direct use of the higher-resolution source data, against which MODIS observations are normally benchmarked (e.g. Rittger et al 2021). This higher resolution allows us to directly isolate the seasonal snowline elevation, rather than snow-covered area, and thus investigate the spatial variations of snow dynamics and their dependence on climate differences between distinct domains. This is particularly valuable due to the complex relationship with variables such as precipitation and its phase, which may be highly modulated by ongoing warming (Jennings et al 2018, Jouberton et al 2022) or the variable presence of the summer monsoon (Mölg et al 2014, Shaw et al 2022).

3.2. SLA variability is controlled by snowfall seasonal partitioning

We leverage catchment-specific results to investigate the climatological factors best explaining the spatial variations of SLA climatology in HMA. Our results highlight that metrics related to precipitation partitioning, rather than temperature itself, show the strongest correlation (0.8) with the spatial variations of SLA climatology (figure 2 and SI figure 6): the annual solid precipitation fraction and the summer

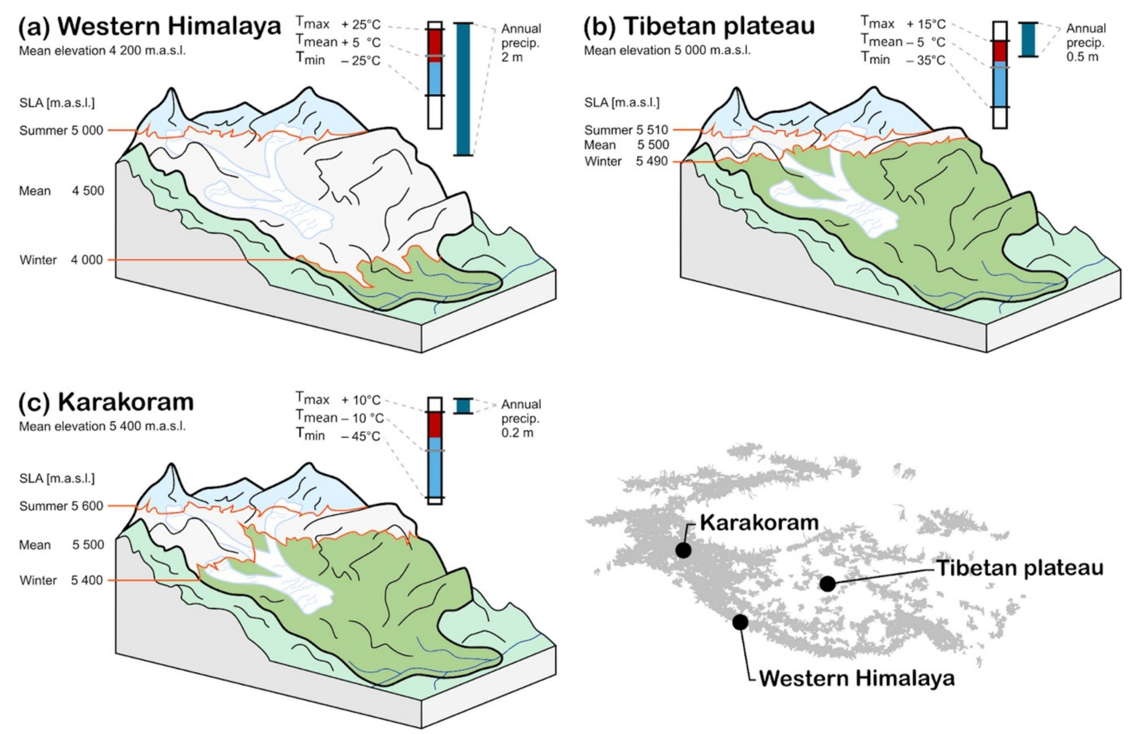

Figure 3. (a)–(c) Conceptual representation of the snow line altitude (orange line) and climatic variables of three catchments of the region. The area permanently covered by snow is indicated in light blue and the area partially covered is in gray.

JJA and spring MAM fractions of annual solid precipitation. The annual solid precipitation fraction is inversely correlated with a_0 (figure 2(d)); this is intuitive, as high solid precipitation fractions at the reference elevation promote lower-elevation snowlines.

Seasonal fraction of solid precipitation shows an even clearer association with the SLA climatology. The JJA fraction of annual snowfall is positively correlated ($\rho = 0.99$) with a_0, while the MAM fraction of snowfall is negatively correlated ($\rho = -0.88$) with a_0 (figure 2 and SI figure 6). Catchments which receive their most extensive snowfall in warm summer months such as in the Central and Eastern Himalaya or parts of the Tibetan Plateau, linked to the monsoonal climate (e.g. Sakai and Fujita 2017), typically exhibit snow cover only at higher-elevations (high a_0), and reduced SLA seasonality (low a_1, figure 3(b)). Catchments which receive extensive snowfall in spring months, on the other hand, accumulate snow at lower elevations (reducing a_0) while also increasing the importance of seasonal snow depletion (higher a_1, figures 3(a) and (c)). In fact, these three elements highlight the interlinkages of precipitation and temperature seasonality to snow dynamics: although across catchments temperature itself is not directly related to SLA variations ($\rho = 0.43$), the annual amplitude of temperature is positively correlated with a_1 ($\rho = 0.82$; SI figure 6). Indeed, the freezing line will vary with temperature, but this also implies that lower annual ranges of temperature variation allow only high-elevation annual-average snowlines (a_0).

The seasonal partitioning of snowfall and the solid fraction of precipitation can be identified as a common control of the spatial variability of SLA, despite its heterogeneity across HMA. These findings confirm that precipitation partitioning is the clearest driver for snow phenological differences across HMA (SI figures 6–10). This is particularly important given that differences in precipitation seasonality can sometimes have a much stronger role in affecting glaciers than differences in total annual precipitation amounts (Maussion *et al* 2014, Sakai and Fujita 2017, Smith and Bookhagen 2018, Jouberton *et al* 2022, Shaw *et al* 2022). Precipitation partitioning remains a major challenge for models and observations alike (e.g. Ding *et al* 2014, Jennings *et al* 2018, Jouberton *et al* 2022, Maina and Kumar 2023) and given forecasted warming in the 21st century, it will play an increasingly critical role in the presence of mountain snow cover and SLA in HMA (Li *et al* 2020, Lalande *et al* 2021, Collier *et al* 2024). Consequently, regional snow models should pay close attention to the interactions of temperature with precipitation for future simulations.

3.3. Influence of orography on SLA variability along the margins of HMA

We extend this analysis to examine the SLA variability across the principal topographic divides of HMA,

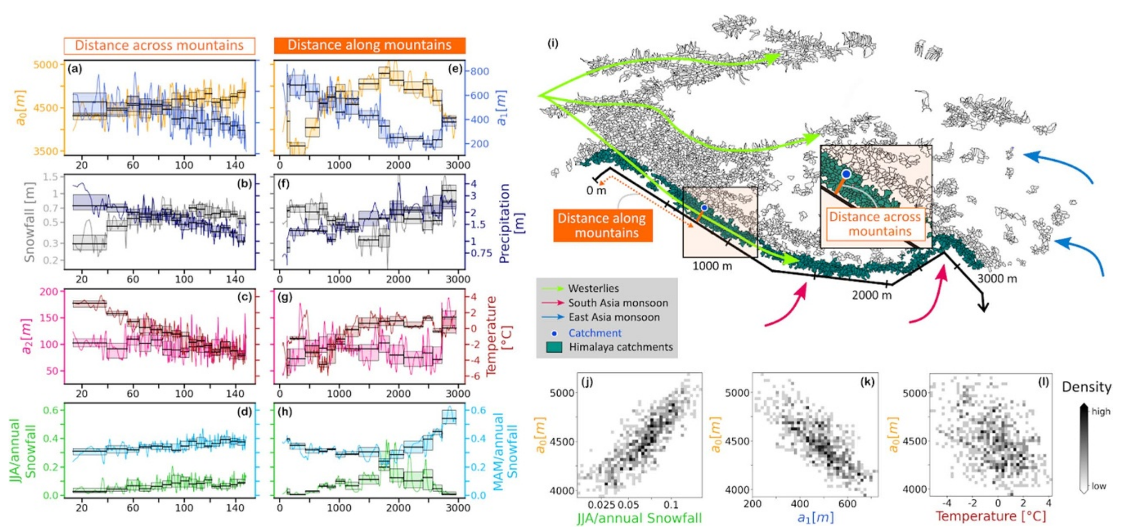

Figure 4. (a)–(h) Across and along-range variability of different SLA and climatic variables for catchments in the Hindu Kush–Karakoram–Himalayan (HKH) mountain chain (i). (i) Catchment map with the HKH catchments colored in green. (j)–(l) Density scatter plots of a_0 as a function JJA/annual snowfall ratio, a_1 and temperature for the HKH catchments. The corresponding Spearman coefficients are (j) 0.84, (k) −0.75, (l) −0.42. Please see also SI figures 11 and 12 for corresponding depictions of the Kunlun–Altun Shan and Tien Shan mountain chains.

where climatic gradients are strongest, glaciers are most common, and topography modifies climatic patterns and resultant snow accumulation (Bookhagen and Burbank 2010, Maussion *et al* 2014, Potter *et al* 2018, Lalande *et al* 2023). The monsoonal-influence decreases across the Himalayas because of the orography: total precipitation and temperature decrease with elevation (figures 4(a)–(h)) and JJA/annual and MAM/annual snowfall show little variation (figures 4(d) and (h)). This relative change in the influence of the monsoon has a clear effect on a gradual increase of a_0 and a decrease of a_1. Along mountains from west (0 km) to the mid-Himalayas (∼1800 km—figure 4(i)), the south monsoonal influence increases and reaches a peak while westerlies become less dominant, reflecting an inverse relationship between JJA/annual and MAM/annual snowfall fractions (figures 4(d) and (h)). As a result, a_0 increases from 3500 m to 5500 m and a_1 decreases from 800 m to 200 m on this western portion of the along-mountains distance (figure 4(e)). Then, on the second portion (from 1800 km to 3000 km), the SLA parameters switch to the opposite trend, linked to a decreasing South but increasing East Asian monsoon influence. This local analysis highlights that the same principle controls are in play for the Hindu Kush–Karakoram–Himalaya range as across the broader region (figures 2 and 3(j–l)). Once again snowfall and precipitation partitioning metrics, highly influenced by macroscale climate patterns and their regional extents (e.g. the strength and intrusion of the summer monsoon), exert a clear control on both local and regional spatial variability of SLA (Bookhagen and Burbank 2010, Nash *et al* 2024). Similarly, for the Tien Shan (SI figure 11) and Kunlun–Altun Shan (SI figure 12) mountain chains, we find again that snowfall (including seasonality) and precipitation partitioning metrics exhibit the strongest correlations with SLA phenology (SI text 1). Catchment temperature plays a secondary role in the Kunlun–Altun Shan, and shows no correlation in the Tien Shan.

3.4. Contrasting 21st century changes in SLA between the East and the West of HMA

Previous analyses have struggled to find clear trends due to the high interannual variability of snow metrics in HMA subregions (You *et al* 2020, Li *et al* 2022, Tang *et al* 2022, Ren *et al* 2024). Our comparison of the first two decades of SLA variations in the 21st century based on high resolution satellite imagery highlights several contrasting patterns of seasonal changes. The western regions of HMA (Pamir, Karakoram, Western Himalaya) have undergone increased snow coverage, expressed as seasonal SLA decrease, in spring and summer (−61 ± 79 m, −36 ± 80 m, −62 ± 88 m change in MAM averaged over the respective regions ± the standard deviation, −32 ± 100 m, −29 ± 96 m, −48 ± 158 m in JJA, SI table 1). On the contrary, there is a widespread increase in SLA in autumn (September–October–November, SON) across the region, and especially Nyainqentanglha, Hengduan Shan and South-East Himalaya (+40 ± 78 m, +30 ± 120 m and +44 ± 127 m change in SON respectively, SI table 1 and figure 5). This corroborates previous observations that have indicated significant shortening of snow cover duration in Nyainqentanglha and Tien Shan, and increase in the Pamir, Karakoram and

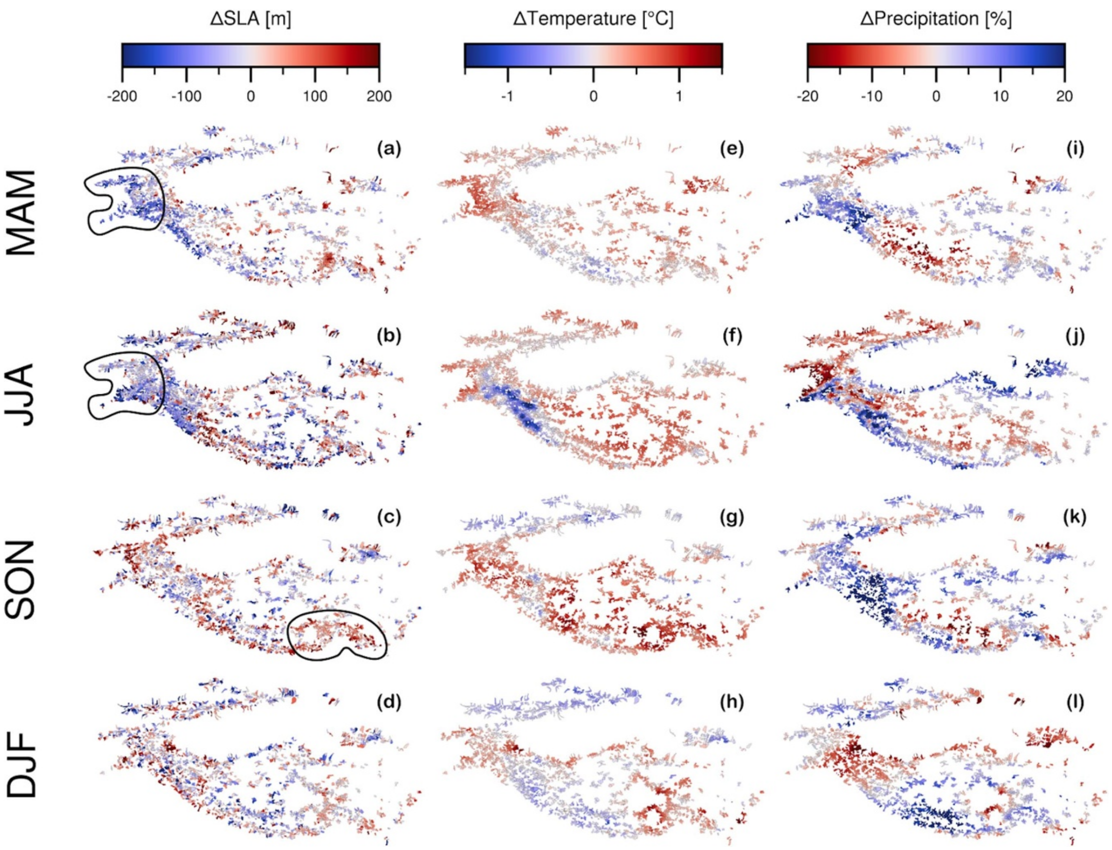

Figure 5. Mean seasonal SLA (a)–(d), temperature (e)–(h) and precipitation (i)–(l) changes between the 1999–2009 and 2009–2019 decades. Changes in mean precipitation are expressed as the percent change from 2009–2019 to1999–2009. The Pamir region is circled in black on the panels (a)–(b) and the Nyainqentanglha region on the panel (c).

Western Himalaya regions (Tang *et al* 2022). Notably, both of these patterns are accompanied by a general increase in air temperature, especially in autumn and summer, except for parts of the Pamir (no temperature change) and Karakoram (cooling) regions in summer. The climatology suggests complex regional changes in seasonal precipitation, with precipitation increases in the Pamir and Karakoram in the spring and, more broadly, in the autumn (figure 5, Jiang *et al* 2023). Precipitation increases are evident along the Western and Central Himalayas, as well as along the Kunlun–Altun Shan, in the summer and autumn, whereas the Tibetan Plateau shows increased precipitation in autumn and winter. The Tien Shan exhibits a variety of precipitation patterns due to the complexity of local meteorology (e.g. Barandun *et al* 2021).

The temperature and precipitation patterns do not show a direct control on SLA changes (figure 5), but there is a clear correspondence between the spring and early summer snowline evolution (figure 6(c)) and the winter precipitation (figure 6(e)). For the western regions (Pamir and Karakoram especially), more snow in the winter results in lower SLA in the spring and early summer, as well as a later peak in SLA (figures 6(b) and (g)). In these regions the SLA is not sensitive to increasing winter temperature as they remain far below the freezing line (figure 6(g)). There, the longer-lasting snowpack could, in fact, be partly responsible for the late spring and early summer decline in air temperature (figure 5(f), Wang *et al* 2018). In the eastern regions of South–East Himalaya and Nyainqentanglha, the increase in temperature particularly in spring and autumn renders the changes in total precipitation secondary, by controlling precipitation phase and snow cover retention, leading to a general increase in SLA particularly in these seasons (figure 6(h)). Despite a lower-elevation and longer-lasting snowpack in the West in the spring and early summer (figure 6(b)), the entire region undergoes rising SLA in the late summer and early autumn (figure 6(d)), indicating that these seasons are more sensitive to the rising air temperatures (figure 6(f)) than to the winter snowfall changes.

Our observed SLA changes correspond well to the geodetic mass balance and albedo patterns of glaciers observed over the period 2000–2020 (Hugonnet *et al* 2021, Ren *et al* 2024), indicating that glaciers undergo a similar response to regional climate changes. In particular, the albedo of glaciers has increased in the west in spring and summer, while it

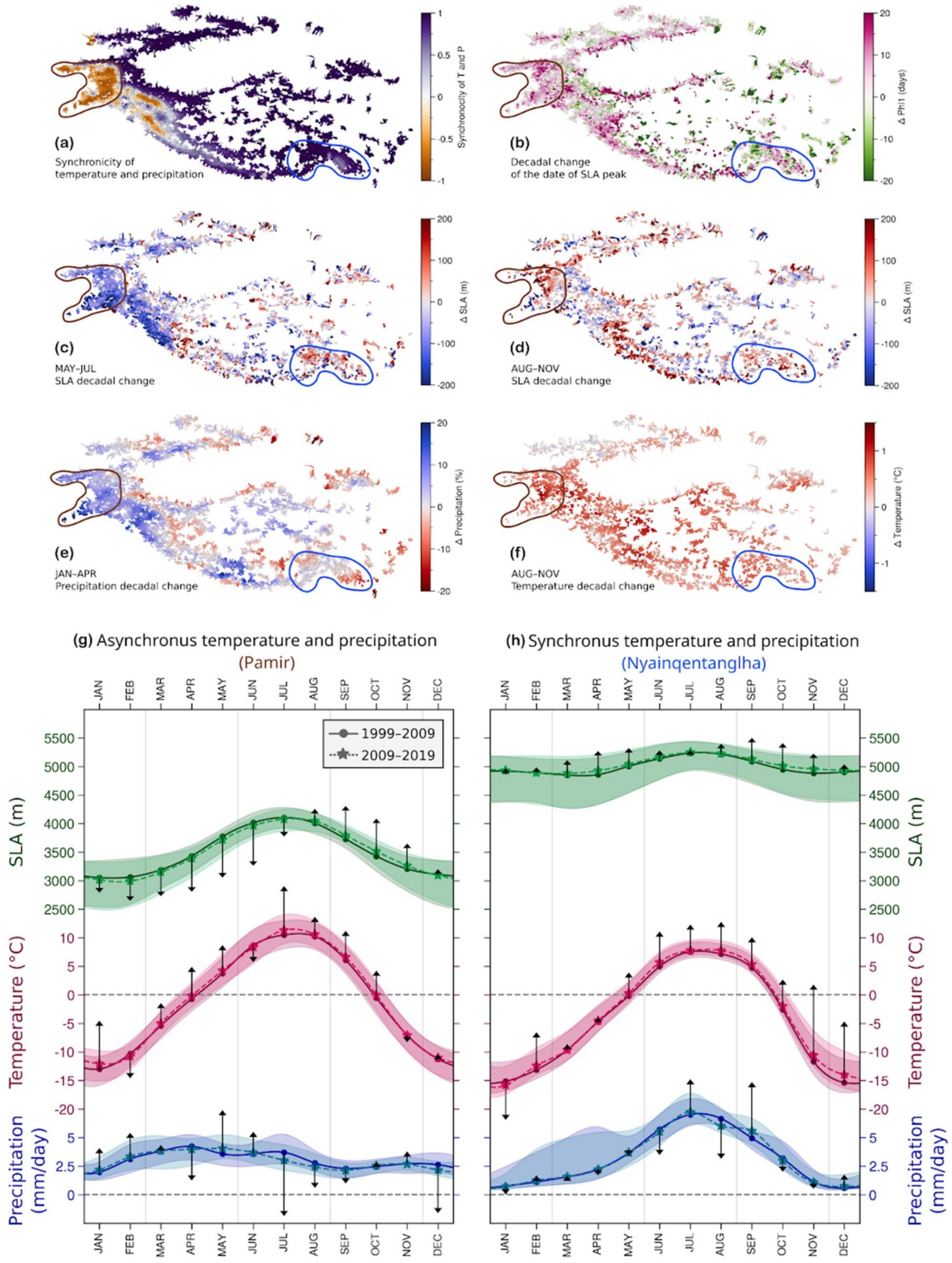

Figure 6. (a) Synchronicity of temperature and precipitation, defined as the Spearman's coefficient between monthly mean air temperature and precipitation values. A Spearman's coefficient of $+1$ means a complete synchronicity of T and P annual variations, whereas a value of -1 denotes an independent evolution of T and P over the period 1999–2019. (b)–(f) Changes between the 1999–2009 and 2009–2019 decades of: (b) harmonic coefficient Φ_1 standing for the date of SLA peak (a negative value indicates that the SLA peak is happening sooner in the recent decade), (c) mean SLA over the months May to July, (d) mean SLA over the months August to November, (e) total precipitation received from January to April and (f) mean temperature over the months August to November. (g)–(h) Mean SLA, temperature and precipitation decadal changes between 1999–2009 and 2009–2019 for the Pamir and Nyainqentanglha regions. The arrows indicate the monthly sign and relative proportion of the variation observed. The shaded areas correspond to the $1-\sigma$ spread over the region. The Pamir region is circled in brown and the Nyainqentanglha region in blue on the panels (a)–(f).

has decreased everywhere else and in all other seasons (Ren *et al* 2024). Similarly, the Pamir, Karakoram and Kunlun regions demonstrated near-neutral glacier mass balances during this period, while glaciers are losing mass extensively in all other regions (Hugonnet *et al* 2021). Two regional trends are therefore visible in HMA during the 1999–2019 period: (1) In the west, higher winter snowfall results in a longer-lasting snowpack and lower SLA in spring and early summer (figures 5(a) and (b)) possibly leading to albedo driven and/or density driven (katabatic wind) summer cooling (figure 5(f)) which could have promoted a feedback toward a pattern of reduced mass loss (Farinotti *et al* 2020, Ren *et al* 2024). (2) In the east, a weakening summer monsoon combined with warming air temperature result in rising SLA and exacerbating declining glacier health (Miles *et al* 2021, Shaw *et al* 2022). This confirms the important link between the state of the spring and early summer snowpack and glacier health, although the generalized increase in summer and autumn temperatures limit this effect, leading to recent rising autumn SLA and glacier decline throughout the entire region (Hugonnet *et al* 2021, Ren *et al* 2024, Xie *et al* 2024).

3.5. Limitations

The greatest limitations of our approach come from the cloud cover preventing snowline identification in the optical satellite images, along with the variable frequency of image acquisitions throughout the study period. Although we expect these elements to have a limited influence on our analysis of the regional trends and drivers of SLA (Sasaki *et al* 2024), promising lines of research on sensor fusion (e.g. Rittger *et al* 2021), including with Synthetic Aperture Radar sensors, could reduce potential biases of future studies. Such studies will also benefit from longer records of earth observation data as well as from improved resolution and physics of climate reanalysis and atmospheric models (e.g. Collier *et al* 2024) that may further constrain the degree to which precipitation phase changes drive patterns of SLA response. Despite these limitations, the SLA patterns we quantified are robust and provide opportunities for both catchment and regional scale hydrological modeling through data assimilation (e.g. Metref *et al* 2023) and model validation (e.g. Buri *et al* 2023, Fugger *et al* 2024).

4. Conclusions

We calculated the SLA seasonality of all catchments in HMA for the period 1999–2019. Our results have shown a high spatial variability in the mean SLA and its seasonal patterns, with lower mean SLA in the southern and western periphery catchments, which is also where the yearly altitudinal amplitude of the snowline is the greatest. The catchment SLA is primarily controlled by the precipitation phase, in terms of the seasonal partitioning of precipitation and its phase rather than strictly with temperature itself, which highlights the influence of the different climatic regimes on the state of the snowpack and its evolution. In the monsoon-dominated catchments where most of the snowfall occurs during the monsoon, the mean SLA is higher, while in the westerlies-dominated catchments, a high spring snowfall ratio leads to lower SLA and higher seasonal variability. These regional differences also lead to different responses to recent climatic changes. In the monsoon-dominated catchments, rises in temperature in the spring and autumn have led to a reduction in the snowfall partition and therefore rising SLA in these seasons. In the west, higher precipitation in winter and early spring has resulted in snow retention in spring and early summer. This precedes cooler air temperatures in summer, suggestive of a cooling effect from this longer-lasting snowpack, the combination of which could have contributed to maintaining glaciers in a near neutral mass balance in this region. However, the generalized rising temperatures limit this effect to spring and early summer and result in a region-wide increase in SLA in summer and autumn.

Data availability statement

The data (catchment SLA and derived metrics) and codes that support the findings of this study are openly available at the following URL/DOI: https://zenodo.org/records/15223344.

Acknowledgments

This work was supported by the SNSF (Science and Swiss National Science Foundation)-SSSTC (Sino-Swiss Science and Technology Cooperation) Project (IZLCZ0_189890) 'Understanding snow, glacier and rivers response to climate in High Mountain Asia (ASCENT)', by the JSPS (Japan Society for the Promotion)-SNSF Bilateral Programmes project (HOPE, High-elevation precipitation in High Mountain Asia; Grant 183633), and the European Research Council (ERC) under the European Union's Horizon 2020 research and innovation program (RAVEN, Rapid mass losses of debris-covered glaciers in High Mountain Asia; Grant 772751). Marin Kneib acknowledges funding from the SNSF Postdoc.Mobility program (Grant No. P500PN_210739).

Conflict of interest

The authors declare that there are no conflicts of interest in the submission of this work.

Ethics statement

The authors declare that there are no ethical issues rising from this work.

ORCID iDs

M Bernat https://orcid.org/0000-0003-3591-7962

E S Miles https://orcid.org/0000-0001-5446-8571
M Kneib https://orcid.org/0000-0002-2420-0475
K Fujita https://orcid.org/0000-0003-3753-4981

References

Ackroyd C, Skiles S M, Rittger K and Meyer J 2021 Trends in snow cover duration across river basins in High Mountain Asia from daily gap-filled MODIS fractional snow covered area *Front. Earth Sci.* **9** 713145

Aranda F, Medina D, Castro L, Ossandón Á, Ovalle R, Flores R P and Bolaño-Ortiz T R 2023 Snow persistence and snow line elevation trends in a Snowmelt-Driven Basin in the Central Andes and their correlations with hydroclimatic variables *Remote Sens.* **15** 5556

Arndt A and Schneider C 2023 Spatial pattern of glacier mass balance sensitivity to atmospheric forcing in High Mountain Asia *J. Glaciol.* **69** 1616–33

Barandun M, Huss M, Usubaliev R, Azisov E, Berthier E, Kääb A, Bolch T and Hoelzle M 2018 Multi-decadal mass balance series of three Kyrgyz glaciers inferred from modelling constrained with repeated snow line observations *Cryosphere* **12** 1899–919

Barandun M, Pohl E, Naegeli K, McNabb R, Huss M, Berthier E, Saks T and Hoelzle M 2021 Hot spots of glacier mass balance variability in Central Asia *Geophys. Res. Lett.* **48** e2020GL092084

Bookhagen B and Burbank D W 2010 Toward a complete Himalayan hydrological budget: spatiotemporal distribution of snowmelt and rainfall and their impact on river discharge *J. Geophys. Res.* **115** F3

Bouamri H, Kinnard C, Boudhar A, Gascoin S, Hanich L and Chehbouni A 2021 MODIS does not capture the spatial heterogeneity of snow cover induced by solar radiation *Front. Earth Sci.* **9** 640250

Buri P *et al* 2023 Land surface modeling in the Himalayas: on the importance of evaporative fluxes for the water balance of a high-elevation catchment *Water Resour. Res.* **59** e2022WR033841

Collier E *et al* 2024 The first ensemble of kilometer-scale simulations of a hydrological year over the third pole *Clim. Dyn.* **62** 7501–18

Ding B, Yang K, Qin J, Wang L, Chen Y and He X 2014 The dependence of precipitation types on surface elevation and meteorological conditions and its parameterization *J. Hydrol.* **513** 154–63

Farinotti D, Immerzeel W W, de Kok R J, Quincey D J and Dehecq A 2020 Manifestations and mechanisms of the Karakoram glacier Anomaly *Nat. Geosci.* **13** 8–16

Fugger S *et al* 2024 Hydrological regimes and evaporative flux partitioning at the climatic ends of High Mountain Asia *Environ. Res. Lett.* **19** 044057

Girona-Mata M, Miles E S, Ragettli S and Pellicciotti F 2019 High-resolution snowline delineation from Landsat imagery to infer snow cover controls in a Himalayan catchment *Water Resour. Res.* **55** 6754–72

Hamm A, Arndt A, Kolbe C, Wang X, Thies B, Boyko O, Reggiani P, Scherer D, Bendix J and Schneider C 2020 Intercomparison of gridded precipitation datasets over a sub-region of the Central Himalaya and the Southwestern Tibetan Plateau *Water* **12** 3271

Hollstein A, Segl K, Guanter L, Brell M and Enesco M 2016 Ready-to-use methods for the detection of clouds, cirrus, snow, shadow, water and clear sky pixels in Sentinel-2 MSI images *Remote Sens.* **8** 666

Hu Z, Dietz A J and Kuenzer C 2019 Deriving regional snow line dynamics during the ablation seasons 1984–2018 in European Mountains *Remote Sens.* **11** 933

Hugonnet R *et al* 2021 Accelerated global glacier mass loss in the early twenty-first century *Nature* **592** 726–31

Immerzeel W W *et al* 2020 Importance and vulnerability of the world's water towers *Nature* **577** 364–9

Immerzeel W W, Wanders N, Lutz A F, Shea J M and Bierkens M F P 2015 Reconciling high-altitude precipitation in the upper Indus basin with glacier mass balances and runoff *Hydrol. Earth Syst. Sci.* **19** 4673–87

Jennings K S, Winchell T S, Livneh B and Molotch N P 2018 Spatial variation of the rain–snow temperature threshold across the Northern Hemisphere *Nat. Commun.* **9** 1148

Jiang J, Zhou T, Qian Y, Li C, Song F, Li H, Chen X, Zhang W and Chen Z 2023 Precipitation regime changes in High Mountain Asia driven by cleaner air *Nature* **623** 544–9

Jouberton A, Shaw T E, Miles E, McCarthy M, Fugger S, Ren S, Dehecq A, Yang W and Pellicciotti F 2022 Warming-induced monsoon precipitation phase change intensifies glacier mass loss in the southeastern Tibetan Plateau *Proc. Natl Acad. Sci.* **119** e2109796119

Khanal S, Tiwari S, Lutz A F, Hurk B V D and Immerzeel W W 2023 Historical climate trends over High Mountain Asia Derived from ERA5 reanalysis data *J. Appl. Meteorol. Climatol.* **62** 263–88

Klein A G and Isacks B L 1999 Spectral mixture analysis of Landsat thematic mapper images applied to the detection of the transient snowline on tropical Andean glaciers *Glob. Planet. Change* **22** 139–54

Kraaijenbrink P D A, Stigter E E, Yao T and Immerzeel W W 2021 Climate change decisive for Asia's snow meltwater supply *Nat. Clim. Change* **11** 591–7

Krajčí P, Holko L, Perdigão R A and Parajka J 2014 Estimation of regional snowline elevation (RSLE) from MODIS images for seasonally snow covered mountain basins *J. Hydrol.* **519** 1769–78

Kumar M, Hodnebrog Ø, Sophie Daloz A, Sen S, Badiger S and Krishnaswamy J 2021 Measuring precipitation in Eastern Himalaya: ground validation of eleven satellite, model and gauge interpolated gridded products *J. Hydrol.* **599** 126252

Lalande M, Ménégoz M, Krinner G, Naegeli K and Wunderle S 2021 Climate change in the High Mountain Asia in CMIP6 *Earth Syst. Dyn.* **12** 1061–98

Lalande M, Ménégoz M, Krinner G, Ottlé C and Cheruy F 2023 Improving climate model skill over High Mountain Asia by adapting snow cover parameterization to complex-topography areas *Cryosphere* **17** 5095–130

Lehner B and Grill G 2013 Global river hydrography and network routing: baseline data and new approaches to study the world's large river systems *Hydrol. Process.* **27** 2171–86

Li Q, Yang T, Zhou H and Li L 2019 Patterns in snow depth maximum and snow cover days during 1961–2015 period in the Tianshan Mountains, Central Asia *Atmos. Res.* **228** 14–22

Li Y, Chen Y, Wang F, He Y and Li Z 2020 Evaluation and projection of snowfall changes in High Mountain Asia based on NASA's NEX-GDDP high-resolution daily downscaled dataset *Environ. Res. Lett.* **15** 104040

Li Y, Sun F, Chen Y, Li B, Fang G, Duan W and Xia Q 2022 The continuing shrinkage of snow cover in High Mountain Asia over the last four decades *Sci. Bull.* **67** 2064–8

Lievens H *et al* 2019 Snow depth variability in the Northern Hemisphere mountains observed from space *Nat. Commun.* **10** 4629

Liu Y, Fang Y and Margulis S A 2021 Spatiotemporal distribution of seasonal snow water equivalent in High Mountain Asia from an 18-year Landsat–MODIS era snow reanalysis dataset *Cryosphere* **15** 5261–80

Loibl D, Richter N and Grünberg I 2025 Remote sensing-derived time series of transient glacier snowline altitudes for High Mountain Asia, 1985–2021 *Sci. Data* **12** 103

Machguth H, Paul F, Kotlarski S and Hoelzle M 2009 Calculating distributed glacier mass balance for the Swiss Alps from regional climate model output: a methodical description and interpretation of the results *J. Geophys. Res. Atmos.* **114** D19

Maina F Z and Kumar S V 2023 Diverging trends in rain-on-snow over High Mountain Asia *Earth's Future* **11** e2022EF003009

Matthews T *et al* 2020 Going to extremes: installing the world's highest weather stations on Mount Everest *Bull. Am. Meteorol. Soc.* **101** E1870–90

Maussion F, Scherer D, Mölg T, Collier E, Curio J and Finkelnburg R 2014 Precipitation seasonality and variability over the Tibetan Plateau as resolved by the High Asia Reanalysis *J. Clim.* **27** 1910–27

McFadden E M, Ramage J and Rodbell D T 2011 Landsat TM and ETM+ derived snowline altitudes in the Cordillera Huayhuash and Cordillera Raura, Peru, 1986–2005 *Cryosphere* **5** 419–30

Mernild S H, Pelto M, Malmros J K, Yde J C, Knudsen N T and Hanna E 2013 Identification of snow ablation rate, ELA, AAR and net mass balance using transient snowline variations on two Arctic glaciers *J. Glaciol.* **59** 649–59

Metref S, Cosme E, le Lay M and Gailhard J 2023 Snow data assimilation for seasonal streamflow supply prediction in mountainous basins *Hydrol. Earth Syst. Sci.* **27** 2283–99

Miao C, Immerzeel W W, Xu B, Yang K, Duan Q and Li X 2024 Understanding the Asian water tower requires a redesigned precipitation observation strategy *Proc. Natl Acad. Sci.* **121** e2403557121

Miles E S, Willis I C, Arnold N S, Steiner J and Pellicciotti F 2017 Spatial, seasonal and interannual variability of supraglacial ponds in the Langtang Valley of Nepal, 1999–2013 *J. Glaciol.* **63** 88–105

Miles E, McCarthy M, Dehecq A, Kneib M, Fugger S and Pellicciotti F 2021 Health and sustainability of glaciers in High Mountain Asia *Nat. Commun.* **12** 2868

Mölg T, Maussion F and Scherer D 2014 Mid-latitude westerlies as a driver of glacier variability in monsoonal High Asia *Nat. Clim. Change* **4** 68–73

Muñoz-Sabater J *et al* 2021 ERA5-Land: a state-of-the-art global reanalysis dataset for land applications *Earth Syst. Sci. Data* **13** 4349–83

Nash D, Carvalho L M V, Rutz J J and Jones C 2024 Influence of the freezing level on atmospheric rivers in High Mountain Asia: WRF case studies of orographic precipitation extremes *Clim. Dyn.* **62** 589–607

Nepal B, Bao Q, Wu G, Liu Y, Kadel I and Lamichhane D 2024 Assessing multi-source precipitation estimates in Nepal: a benchmark for sub-seasonal model assessment *J. Geophys. Res. Atmos.* **129** 1–28

Notarnicola C 2020 Observing snow cover and water resource changes in the High Mountain Asia region in comparison with global mountain trends over 2000–2018 *Remote Sens.* **12** 3913

Palazzi E, Mortarini L, Terzago S and von Hardenberg J 2019 Elevation-dependent warming in global climate model simulations at high spatial resolution *Clim. Dyn.* **52** 2685–702

Pekel J-F, Cottam A, Gorelick N and Belward A S 2016 High-resolution mapping of global surface water and its long-term changes *Nature* **540** 418–22

Pfeffer W T *et al* 2014 The Randolph Glacier Inventory: a globally complete inventory of glaciers *J. Glaciol.* **60** 537–52

Potter E R, Orr A, Willis I C, Bannister D and Salerno F 2018 Dynamical drivers of the local wind regime in a Himalayan valley *J. Geophys. Res. Atmos.* **123** 13,186–202

Pritchard H D 2019 Asia's shrinking glaciers protect large populations from drought stress *Nature* **569** 649–54

Rabatel A, Bermejo A, Loarte E, Soruco A, Gomez J, Leonardini G, Vincent C and Sicart J E 2012 Can the snowline be used as an indicator of the equilibrium line and mass balance for glaciers in the outer tropics? *J. Glaciol.* **58** 1027–36

Racoviteanu A E, Rittger K and Armstrong R 2019 An automated approach for estimating snowline altitudes in the Karakoram and Eastern Himalaya from remote sensing *Front. Earth Sci.* **7** 220

Ren S *et al* 2024 Observed and projected declines in glacier albedo across the Third Pole in the 21st century *One Earth* **7** 1587–99

Rittger K, Bormann K J, Bair E H, Dozier J and Painter T H 2021 Evaluation of VIIRS and MODIS snow cover fraction in High-Mountain Asia using Landsat 8 OLI *Front. Remote Sens.* **2** 647154

Ronald Eastman J, Sangermano F, Ghimire B, Zhu H, Chen H, Neeti N, Cai Y, Machado E A and Crema S C 2009 Seasonal trend analysis of image time series *Int. J. Remote Sens.* **30** 2721–6

Sakai A and Fujita K 2017 Contrasting glacier responses to recent climate change in high-mountain Asia *Sci. Rep.* **7** 13717

Sasaki O, Miles E S, Pellicciotti F, Sakai A and Fujita K 2024 Contrasting patterns of change in snowline altitude across five Himalayan catchments *EGUsphere* **2024** 1–19

Shaw T E *et al* 2022 Multi-decadal monsoon characteristics and glacier response in High Mountain Asia *Environ. Res. Lett.* **17** 104001

Smith T and Bookhagen B 2018 Changes in seasonal snow water equivalent distribution in High Mountain Asia (1987–2009) *Sci. Adv.* **4** e1701550

Smith T, Bookhagen B and Rheinwalt A 2017 Spatiotemporal patterns of High Mountain Asia's snowmelt season identified with an automated snowmelt detection algorithm, 1987–2016 *Cryosphere* **11** 2329–43

Spiess M, Huintjes E and Schneider C 2016 Comparison of modelled- and remote sensing- derived daily snow line altitudes at Ulugh Muztagh, northern Tibetan Plateau *J. Mt. Sci.* **13** 593–613

Stillinger T, Roberts D A, Collar N M and Dozier J 2019 Cloud masking for Landsat 8 and MODIS Terra over snow-covered terrain: error analysis and spectral similarity between snow and cloud *Water Resour. Res.* **55** 6169–84

Tadono T, Ishida H, Oda F, Naito S, Minakawa K and Iwamoto H 2014 Precise global DEM generation by ALOS PRISM *ISPRS Ann. Photogramm. Remote Sens. Spatial Inf. Sci.* **II–4** 71–76

Tang Z, Deng G, Hu G, Zhang H, Pan H and Sang G 2022 Satellite observed spatiotemporal variability of snow cover and snow phenology over high mountain Asia from 2002 to 2021 *J. Hydrol.* **613** 128438

Tang Z, Wang J, Li H, Liang J, Li C and Wang X 2014 Extraction and assessment of snowline altitude over the Tibetan plateau using MODIS fractional snow cover data (2001–2013) *J. Appl. Remote Sens.* **8** 084689

Tang Z, Wang J, Li H and Yan L 2013 Spatiotemporal changes of snow cover over the Tibetan plateau based on cloud-removed moderate resolution imaging spectroradiometer fractional snow cover product from 2001 to 2011 *J. Appl. Remote Sens.* **7** 073582

Tang Z, Wang X, Deng G, Wang X, Jiang Z and Sang G 2020 Spatiotemporal variation of snowline altitude at the end of melting season across High Mountain Asia, using MODIS snow cover product *Adv. Space Res.* **66** 2629–45

Viviroli D, Kummu M, Meybeck M, Kallio M and Wada Y 2020 Increasing dependence of lowland populations on mountain water resources *Nat. Sustain.* **3** 917–28

Wang Y, Yang K, Zhou X, Chen D, Lu H, Ouyang L, Chen Y, Zhu L and Wang B 2020 Synergy of orographic drag parameterization and high resolution greatly reduces biases of WRF-simulated precipitation in central Himalaya *Clim. Dyn.* **54** 1729–40

Wang Z, Wu R, Chen S, Huang G, Liu G and Zhu L 2018 Influence of Western Tibetan Plateau summer snow cover on East Asian summer rainfall *J. Geophys. Res. Atmos.* **123** 2371–86

Xiao X and Liang S 2024 Assessment of snow cover mapping algorithms from Landsat surface reflectance data and application to automated snowline delineation *Remote Sens. Environ.* **307** 114163

Xie F *et al* 2024 Retrieval of high-resolution melting-season albedo and its implications for the Karakoram Anomaly *Remote Sens. Environ.* **315** 114438

Yang W, Yao T, Guo X, Zhu M, Li S and Kattel D B 2013 Mass balance of a maritime glacier on the southeast Tibetan Plateau and its climatic sensitivity *J. Geophys. Res. Atmos.* **118** 9579–94

You Q, Wu T, Shen L, Pepin N, Zhang L, Jiang Z, Wu Z, Kang S and AghaKouchak A 2020 Review of snow cover variation over the Tibetan Plateau and its influence on the broad climate system *Earth Sci. Rev.* **201** 103043

Zhou H, Aizen E and Aizen V 2013 Deriving long term snow cover extent dataset from AVHRR and MODIS data: central Asia case study *Remote Sens. Environ.* **136** 146–62

Supplementary Information

Text 1. *SLA variability of the Himalaya, Tien Shan and Kunlun-Altun Shan mountain ranges.*

We consider along- and across- range snow line altitude (SLA) variability around the principal topographic divides of high mountain Asia (HMA) to disentangle the interplay of orography, the primary controls of SLA, and SLA variability (figure 4, SI figures 4 and 5). For all these analyses, we use the altitudinally-corrected catchment-specific ERA5-Land data (Methods), binned by distance along or across the mountain ranges (figure 4).

In the Himalaya (figure 4, text reproduced here from the main text for completeness), the monsoon-influence on climate and SLA decreases across the range because of the orography: total precipitation and temperature decrease with elevation (figure 4(a-h)) and JJA/annual and MAM/annual snowfall show little variation (figure 4(d-h)). This relative change in the influence of the monsoon has a clear effect on a gradual increase of a_0 and decrease of a_1. Along mountains from west (0 km) to the mid-Himalayas (~1 800 km - figure 3(i)), the south monsoonal influence increases and reaches a peak while westerlies become less dominant, reflecting an inverse relationship between JJA/annual and MAM/annual snowfall fractions (figure 3(d-h)). As a result, a_0 increases from 3 500 m to 5 500 m and a_1 decreases from 800 m to 200 m on this western portion of the along-mountains distance (figure 3(e)). Then, on the second portion (from 1 800 km to 3 000 km), the SLA parameters switch to the opposite trend, linked to a decreasing South but increasing East Asian monsoon influence.

In the Tien Shan, a complex mixture of moisture source paths leads to more localized weather conditions (Barandun *et al* 2020), rather than strong and clear seasonal advection (such as via the westerlies or the monsoon). This leads to some disagreement between climate reanalyses (Barandun and Pohl 2023), so our interpretations should be taken with caution. However, a_0 and a_1 are inversely correlated with elevation. For the full region, the annual-average (a_0) and annual amplitude (a_1) of SLA are inversely related (SI figure 8). There is differential response of SLA for the southern and northern portions of the domain, as warmer temperatures in the south (altitudinally-adjusted) force a higher general SLA (a_0) in this domain, but that precipitation phase (using the JJA fraction of annual snowfall) is the best predictor of SLA differences. The east-west patterns are complex due to local weather conditions, and highlight a general decline in a_0 moving eastwards, as catchment elevation decreases. Again, the JJA fraction of annual snowfall is the best overall predictor of a_0, and therefore a_1 (SI figures 5 and 6).

In the Kunlun-Altun Shan domain, SLA metrics are again inversely correlated with elevation, but uniquely in this domain, the ERA5-Land data does not show differentiation of precipitation across the range. Along the mountains, precipitation differentiation highlights the transition of dominant moisture source from westerlies to monsoon, as for the Himalaya (Yao *et al* 2012). As precipitation is held steady across much of the region, in this domain temperature is a secondary predictor of SLA differences, but surprisingly, warmer temperatures relate to a lower mean SLA (a_0). Consequently, this relationship does not correspond to a direct control (warmer temperatures would lead to more melt, as well as more liquid precipitation, and therefore higher snowlines). Rather, it is more likely that these warmer (altitudinally-adjusted) temperatures are actually a proxy for the moisture supply regime, as the temperature is, in this domain, related to the seasonal partition of moisture supply, particularly across the mountain range. In the south, colder (altitudinally-adjusted) temperatures relate to a larger JJA snowfall fraction, indicative of monsoon moisture sourcing, and a higher SLA despite the colder temperatures. As for the other regions, the JJA fraction of snowfall is again the best predictor of SLA variations across the whole mountain range.

Our results show that in all three mountain chains, the JJA fraction of snowfall is the best overall predictor of SLA annual mean (a_0) and annual amplitude (a_1). This is despite very different settings in terms of moisture source and orography: for the Hindu Kush-Himalaya (HKH), summer moisture is driven across the range by the monsoon and winter precipitation comes from the West; for the Tien Shan a variety of local situations lead to multiple source paths without consistent orographic drive; for the Kulun-Altun Shan moisture supply is primarily from westerlies, but with an important component from the monsoon in summer. While SLA is clearly best predicted by seasonal precipitation phase (i.e. the JJA fraction of snowfall), we hypothesize that the intersection of moisture source path and orography controls where peak snowfall occurs. In the Hindu Kush-Himalaya, moisture from the monsoon is directed across the mountains, leading to strong orographic amplification of precipitation (e.g. Bookhagen and Burbank 2010) and a severe gradient across the range, while seasonality of precipitation varies along the range. In the Kunlun-Altun Shan, the monsoon can be an important moisture source in the east, but does not drive across the range, leading to strong orographic effects. The monsoon is instead secondary to the westerlies, which are directed along the range and strongest in the west, leading to differential precipitation along the range, but different precipitation seasonality across the range. This leads to relatively little precipitation quantity differentiation across the range (although the seasonal phase of precipitation does differ) but a strong fluctuation across the range as the moisture supply source transitions. For the Tien Shan, moisture can come from different directions (including local recycling) and there is not a strong local orographic driver or locus of peak snowfall.

Interpreting these patterns in terms of SLA, in the Hindu Kush-Himalaya and the Kunlun-Altun Shan mountain chains, the tradeoff between the monsoons and westerlies is clearly indicated by the seasonality of snowfall (i.e. the JJA fraction of snowfall). This is a direct proxy for precipitation phase, as it accounts for the synchronicity of temperature and precipitation (if they are seasonally in phase or anticorrelated), which is a physical control on SLA. This is despite the generally small fractions of JJA snow relative to the annual total (<0.5). Notably, temperature is only a reliable predictor for SLA metrics across the Kunlun-Altun Shan, where precipitation varies little in quantity but considerably in timing; here, temperature exerts the opposite relationship with SLA to the expected control. In the Tien Shan, despite the variety of sources for summer precipitation, the same relationship of SLA with the JJA fraction of annual snowfall plays out, again despite low total JJA snowfall amounts.

In summary, snowfall and precipitation partitioning metrics, highly influenced by macroscale climate patterns and their regional extents (e.g. the strength and intrusion of the summer monsoon), exert a clear control on both local and regional spatial variability of SLA for all three mountain chains (Bookhagen and Burbank 2010, Nash *et al* 2024). Similarly, we find again that snowfall (and especially snowfall seasonality) and precipitation partitioning metrics exhibit the strongest correlations with SLA phenology. Catchment temperature plays a secondary role only in the Kunlun-Altun Shan, but is in fact a proxy for the transition of the dominant moisture source.

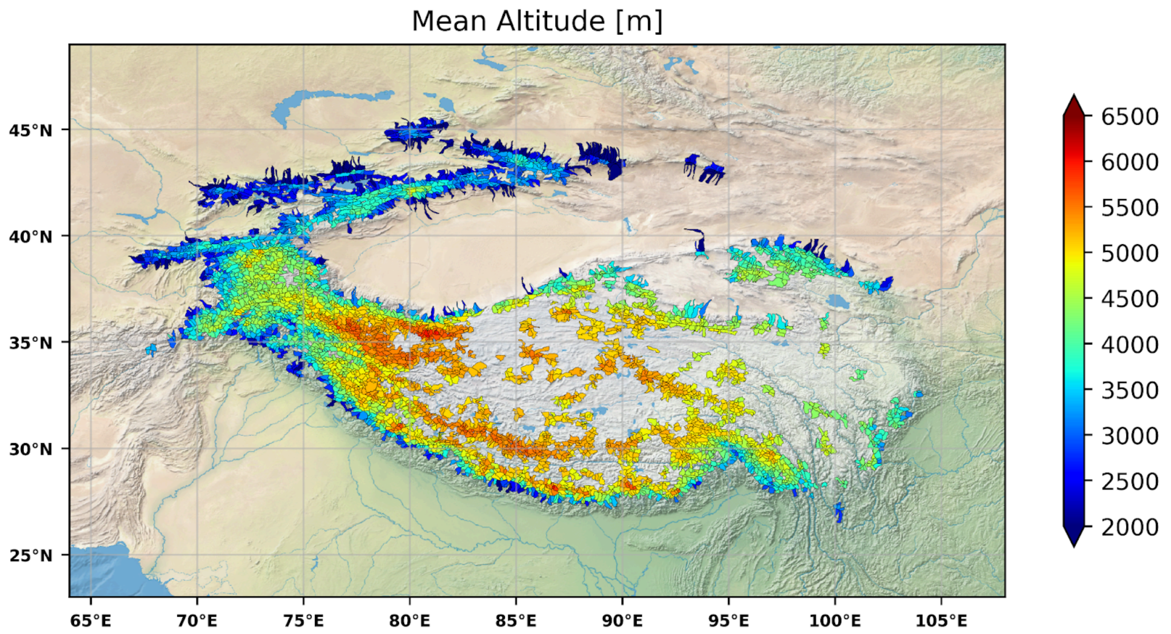

SI Figure 1. *Mean catchment altitude (from SRTM DEM) for the level-9 HydroBASINS catchments in high mountain Asia.*

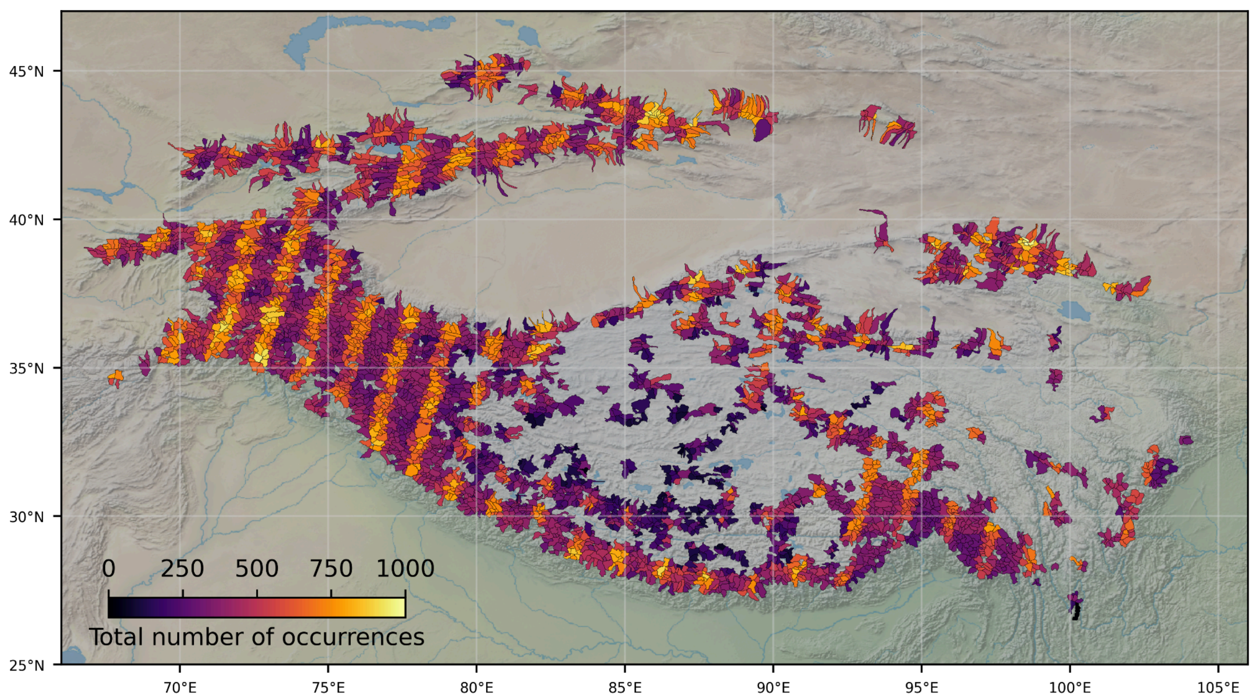

SI figure 2. *Number of available scenes for each catchment over the period 1999-2019 after filtering of clouds.*

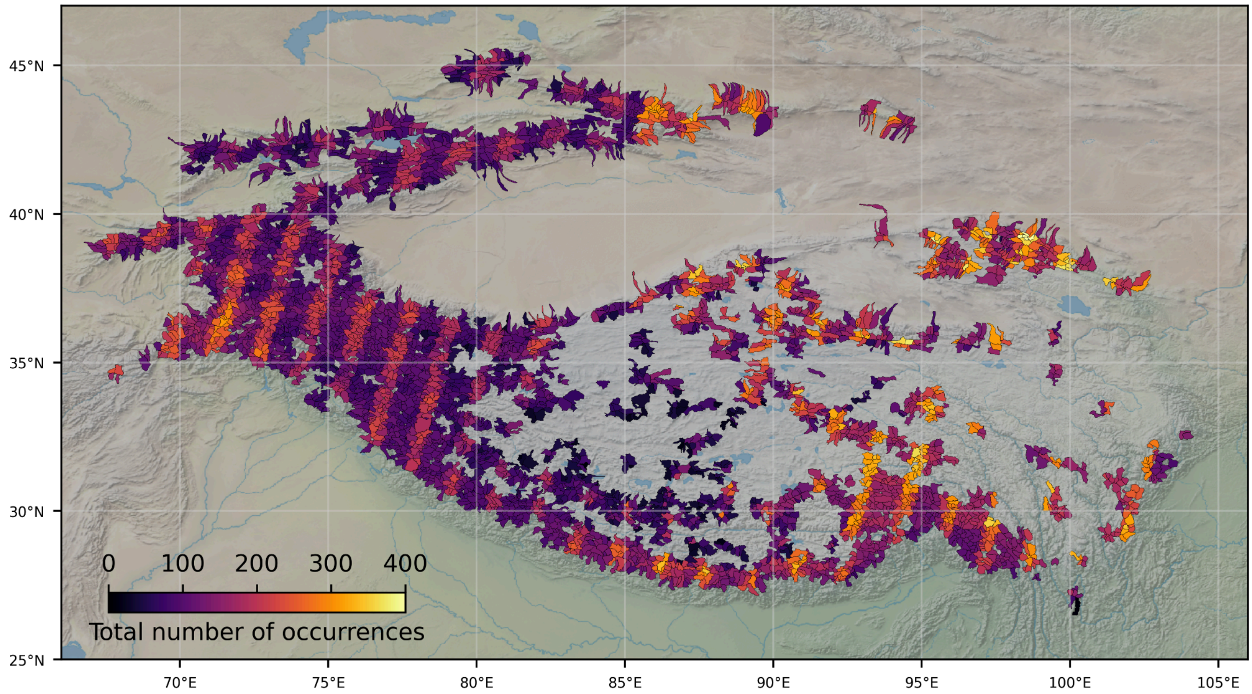

SI figure 3. *Number of available scenes for each catchment over the period 1999-2009 after filtering of clouds.*

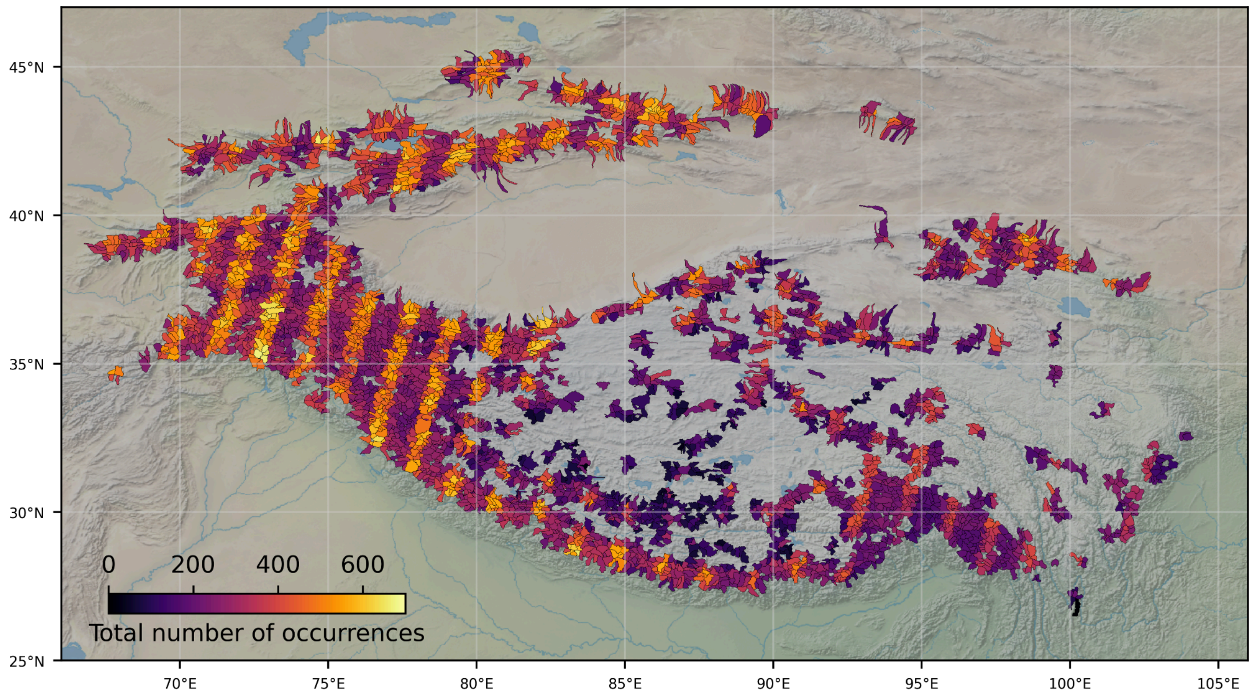

SI figure 4. *Number of available scenes for each catchment over the period 2009-2019 after filtering of clouds.*

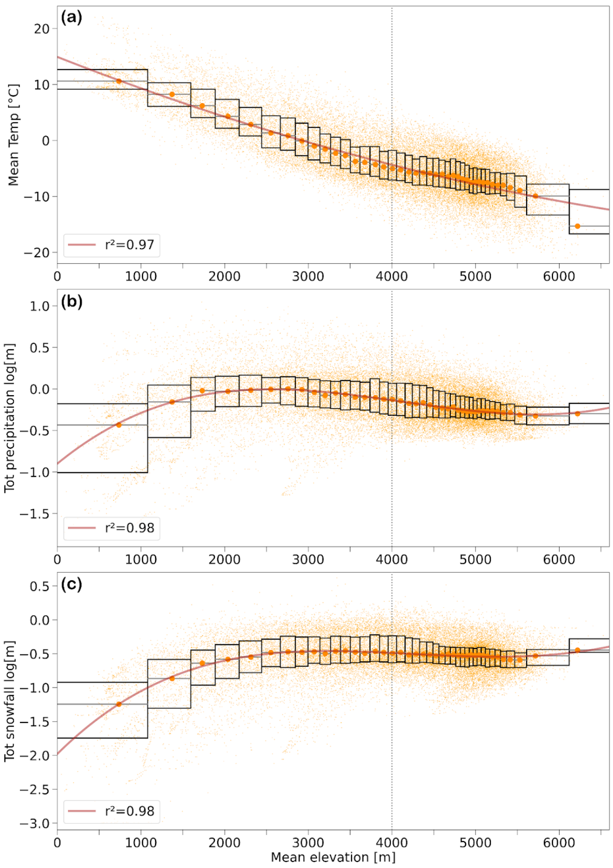

SI figure 5. *Demonstration of altitudinal normalization of temperature (a), precipitation (b) and snowfall (c) data to the reference elevation of 4 000 m a.s.l. (dashed line). Catchment values (yellow scatter plot in background) are first binned with respect to elevation, to reveal the underlying variability (e.g. Machguth et al 2009) (black box plots). Logarithm values of precipitation and snowfall values are used. The median values (orange dots) for each of 40 quantile bins are used to fit a 4th-order polynomial function (red curve). The deviations from this polynomial are then used to normalize each catchment's precipitation values to 4 000 m a.s.l. (dashed vertical grey line).*

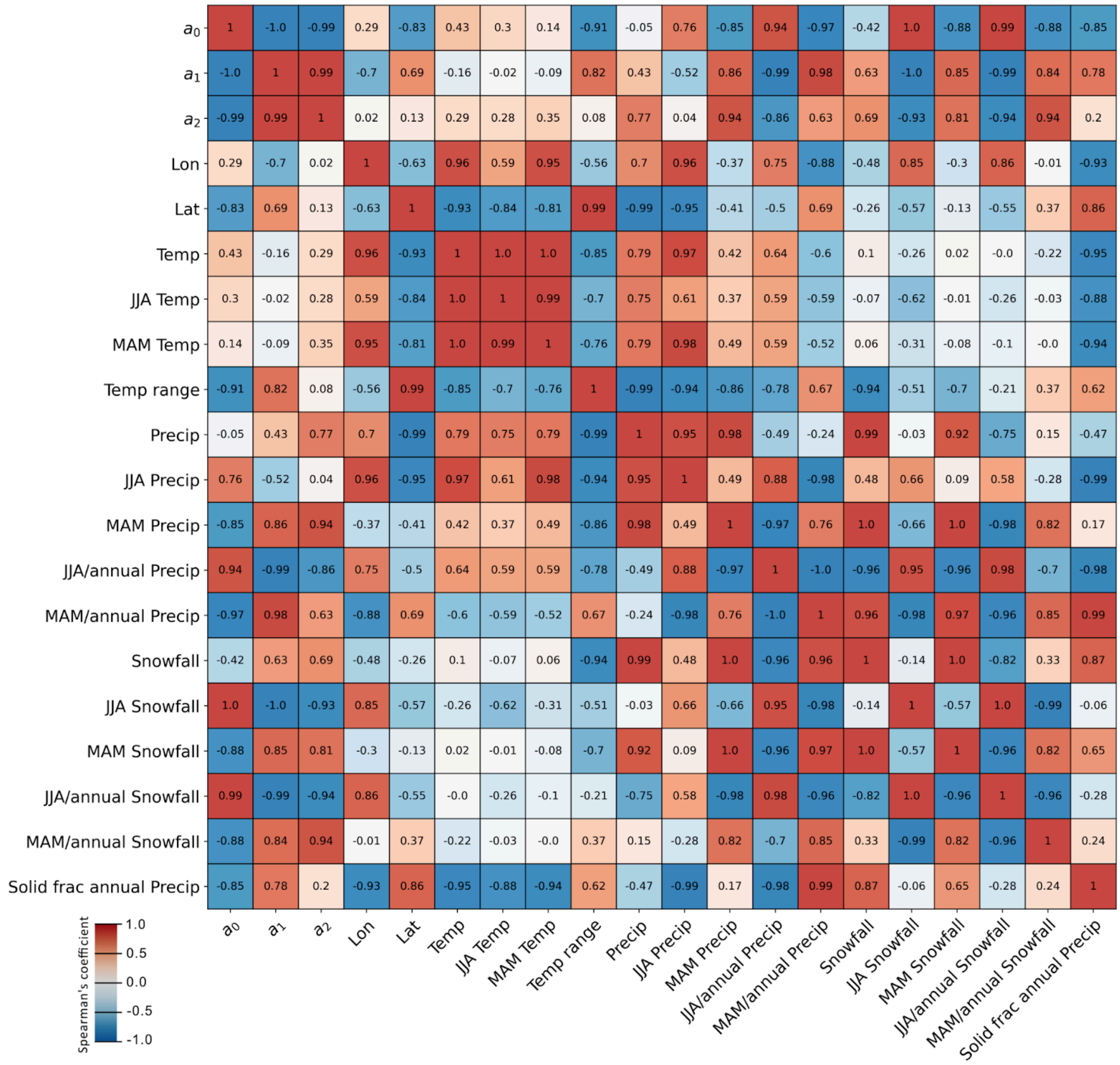

***SI figure 6**. Correlation plot of all variables investigated over the period 1999–2019.*

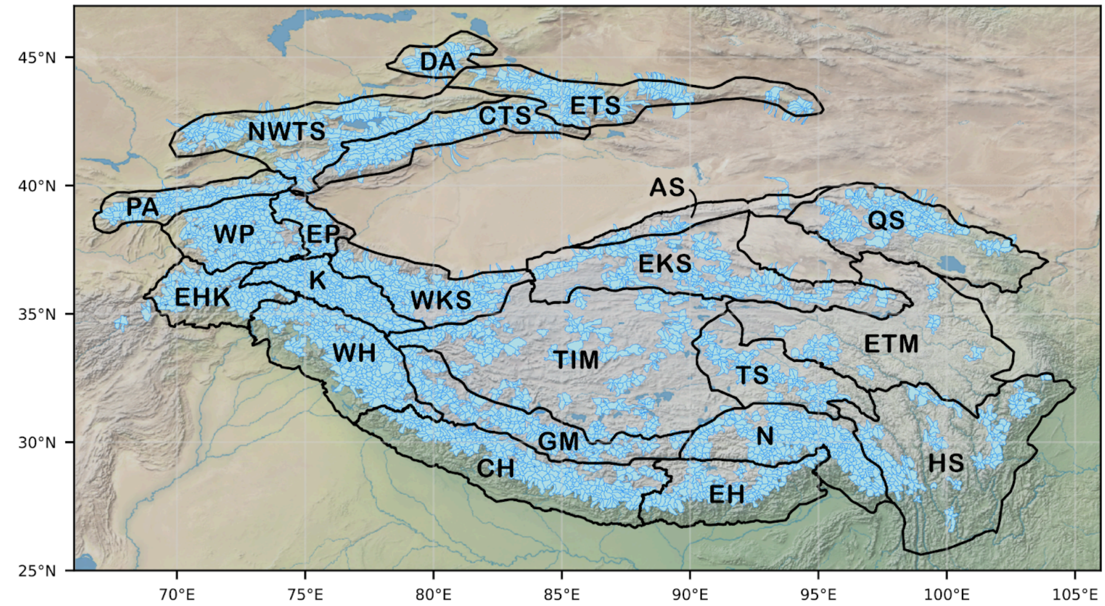

SI figure 7. *High mountain Asia regions (Bolch et al 2019). DA: Dzhungarksy Alatau, ETS: Eastern Tien Shan, CTS: Central Tien Shan, NWTS: North/Western Tien Shan, PA: Pamir Alay, WP: Western Pamir, EP: Eastern Pamir, EHK: Eastern Hindu Kush, K: Karakoram, WH: Western Himalaya, CH: Central Himalaya, EH: Eastern Himalaya, GM: Gangdise Mountains, TIM: Tibetain Interior Mountains, WKS: Western Kunlun Shan, EKS: Eastern Kunlun Shan, AS: Altun Shan, QS: Qilian Shan, EMT: Eastern Tibetan Mountains, TS: Tanggula Shan, N: Nyainqentanglha, HS: Hengduan Shan. The level-9 HydroBASINS catchments in high mountain Asia are indicated in blue.*

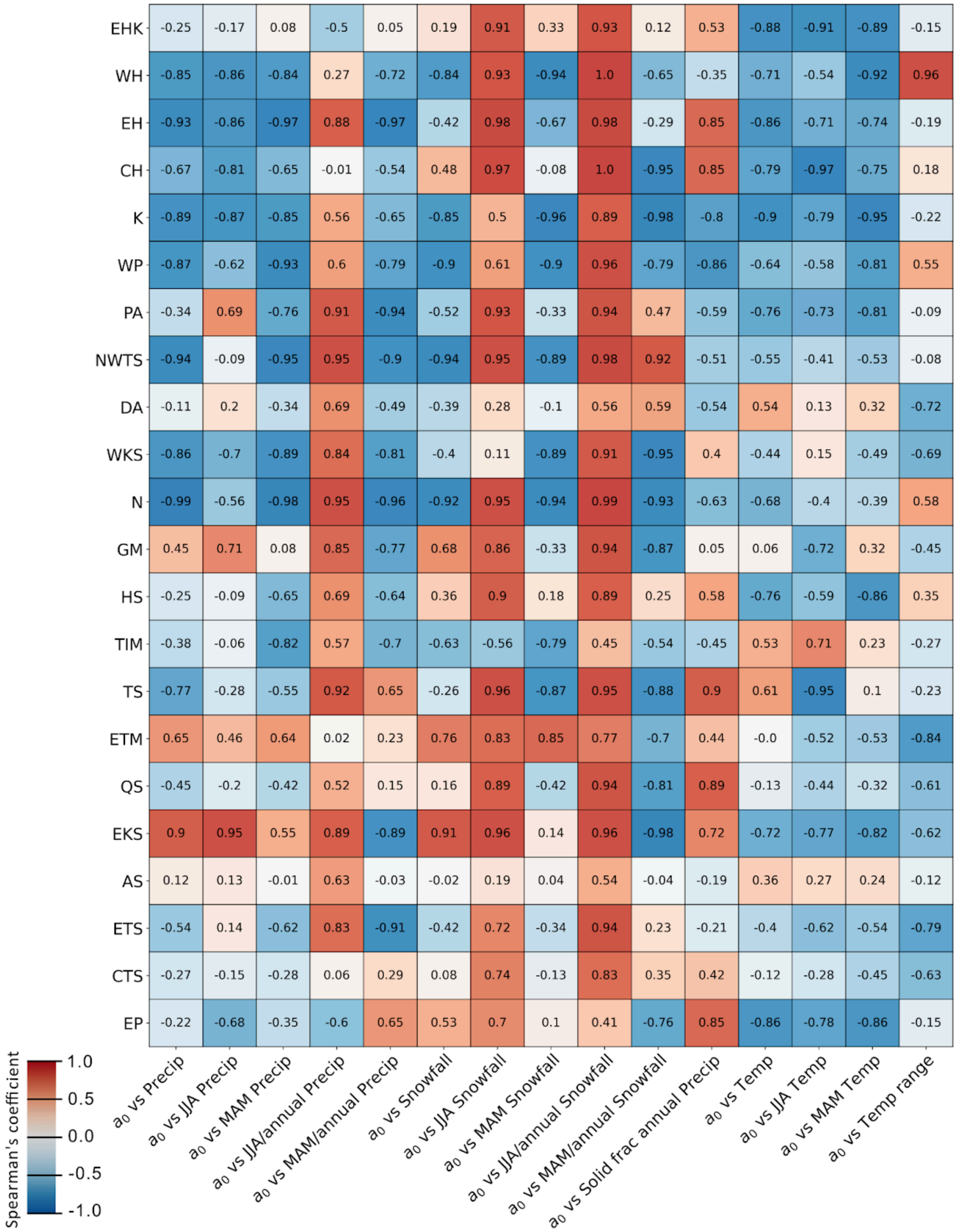

SI figure 8. *Spearman coefficients between the harmonic regression coefficient a_o and the precipitation partitioning indicators for all subregions.*

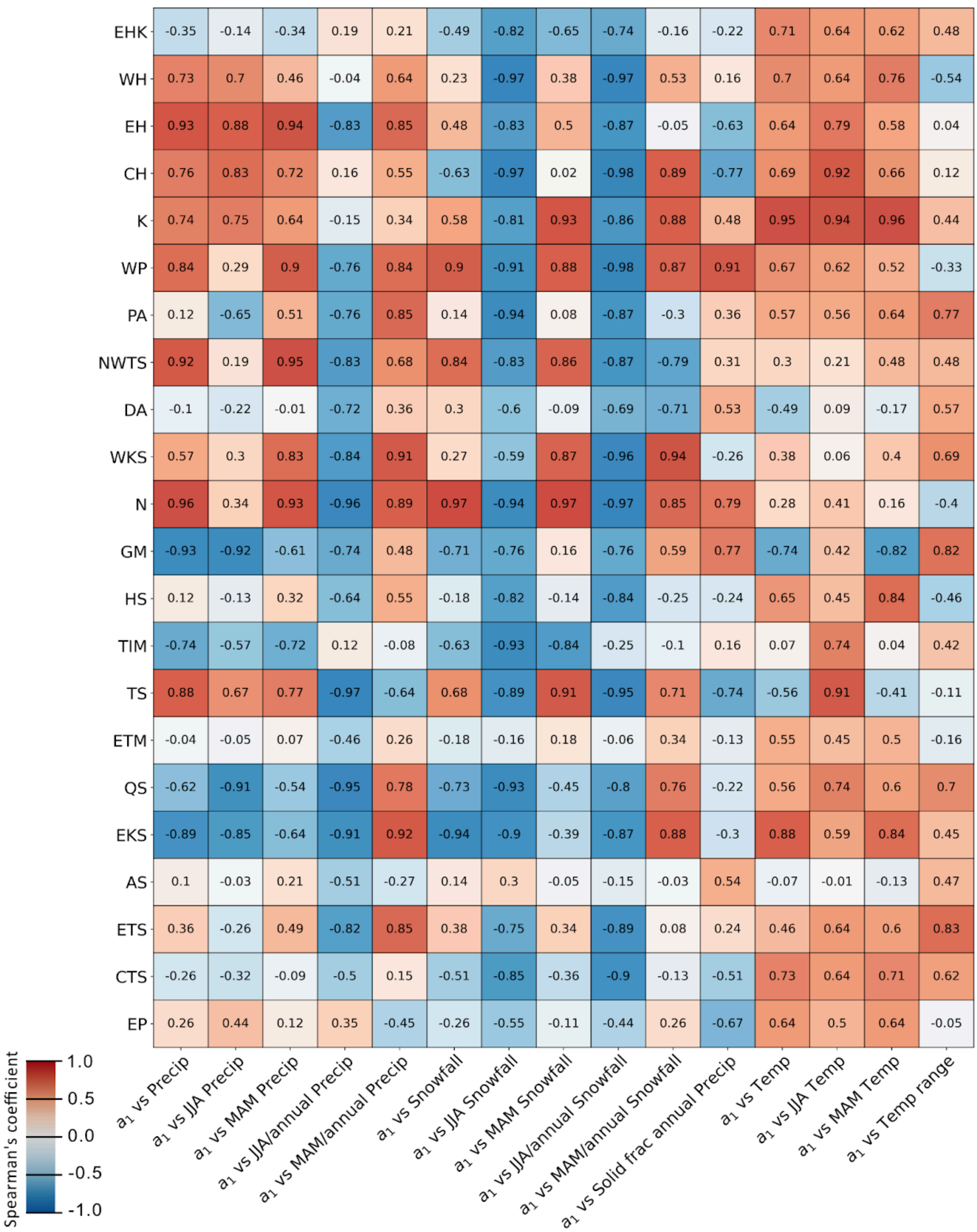

SI figure 9. *Spearman coefficients between the harmonic regression coefficient a_1 and the precipitation partitioning indicators and temperature indicators for all subregions.*

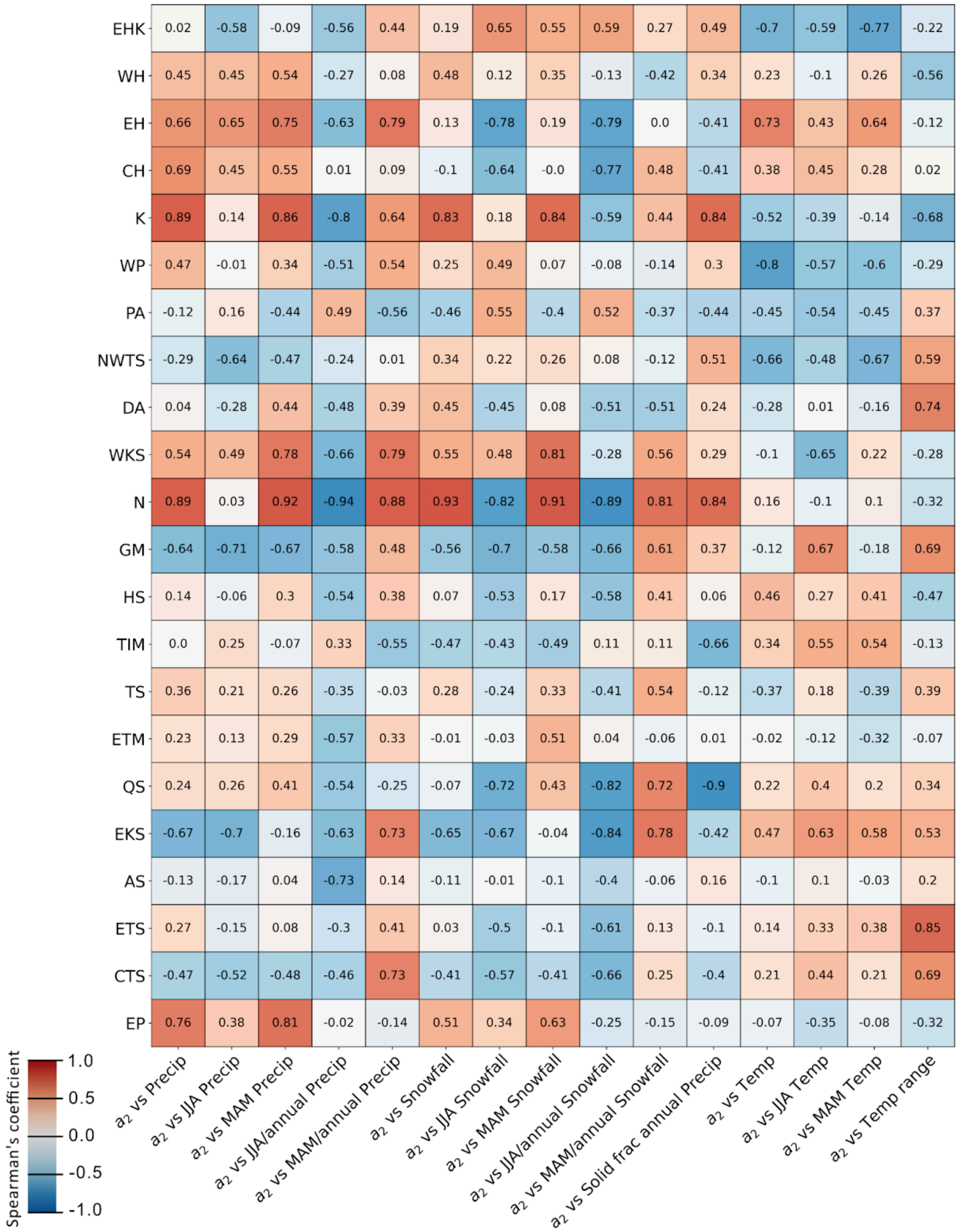

SI figure 10. *Spearman coefficients between the harmonic regression coefficient a_2 and the precipitation partitioning indicators and temperature indicators for all subregions.*

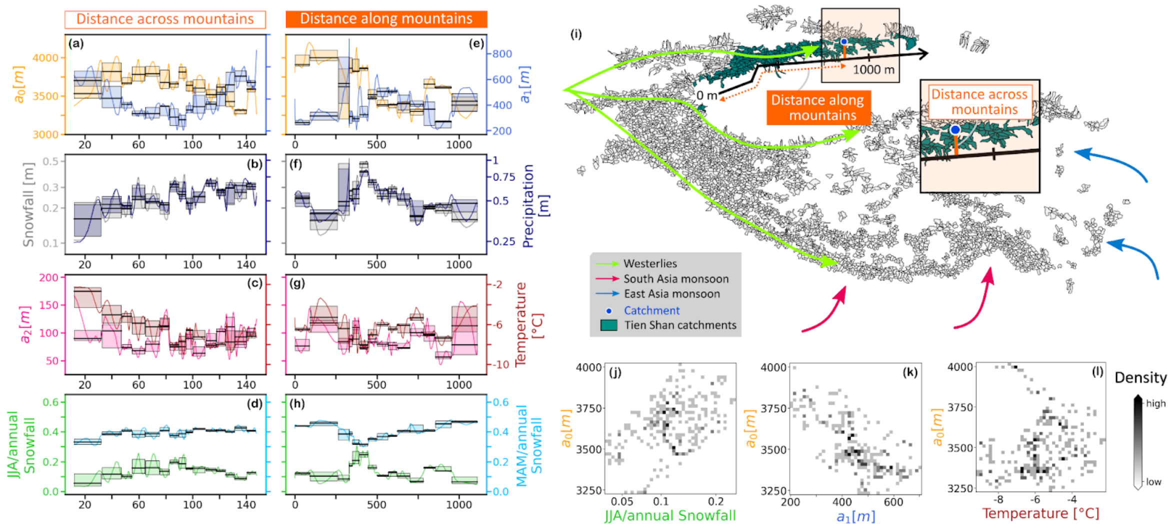

SI figure 11. *(a-h) Across and along-range variability of different SLA and climatic variables for the Tien Shan catchments (i). (i) Catchment map with the Tien Shan catchments colored in green. (j-l) Density scatter plots of a_0 as a function JJA/annual snowfall ratio, a_1 and temperature for the Tien Shan catchments. The corresponding Spearman coefficients are (j) 0.4, (k) -0.71, (l) 0.24.*

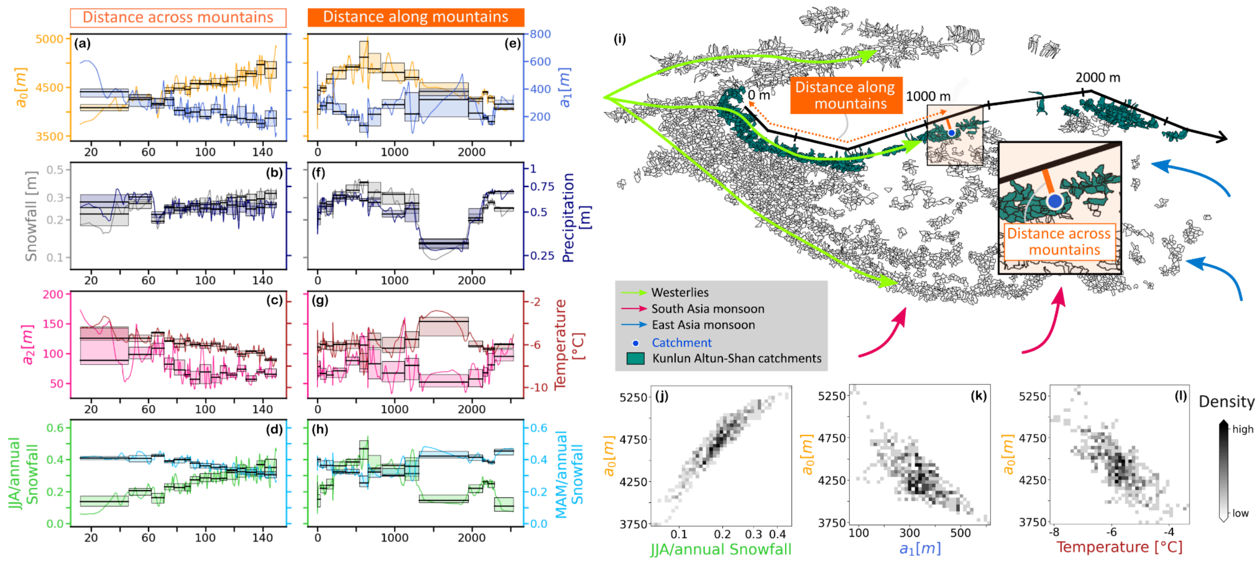

SI figure 12. *(a-h) Across and along-range variability of different SLA and climatic variables for the Kunlun-Altun Shan catchments (i). (i) Catchment map with the Kunlun-Altun Shan catchments colored in green. (j-l) Density scatter plots of a_0 as a function JJA/annual snowfall ratio, a_1 and temperature for the Kunlun-Altun Shan catchments. The corresponding Spearman coefficients are (j) 0.94, (k) -0.70, (l) -0.75.*

SI table 1. *Seasonal SLA changes (m) for each subregion: mean and standard deviation.*

Subregion	SLA change MAM in m (± 1σ)	SLA change JJA in m (± 1σ)	SLA change SON in m (± 1σ)	SLA change DJF in m (± 1σ)
EHK	-89.01 ± 94.47	-79.05 ± 177.07	3.36 ± 125.82	36.21 ± 112.28
WH	-61.57 ± 88.01	-48.65 ± 158.19	1.66 ± 108.41	13.66 ± 118.53
EH	10.38 ± 112.06	-54.1 ± 372.86	44.33 ± 127.13	10.02 ± 67.39
CH	-23.97 ± 110.24	22.22 ± 307.66	37.93 ± 152.82	4.3 ± 92.35
K	-36.04 ± 80.05	-29.34 ± 99.58	-2.8 ± 63.59	-6.06 ± 74.02
WP	-48.62 ± 83.71	-29.3 ± 95.77	24.63 ± 99.12	14.16 ± 113.1
PA	-61.34 ± 79.1	-32.31 ± 99.76	57.25 ± 106.49	-17.21 ± 113.08
NWTS	-24.51 ± 97.32	-35.79 ± 178.75	15.28 ± 126.75	-11.09 ± 143.5
DA	-62.88 ± 267.9	42.34 ± 534.95	-16.22 ± 134.58	-7.31 ± 124.28
WKS	-9.61 ± 95.39	1.33 ± 104.36	20.13 ± 88.01	18.81 ± 84.04
N	32.01 ± 74.33	12.97 ± 177.11	39.67 ± 77.8	9.53 ± 57.04
GM	-12.73 ± 78.96	21.85 ± 193.65	3.42 ± 127.87	-23.52 ± 93.58
HS	51.81 ± 99.28	3.17 ± 251.55	29.83 ± 120.49	23.79 ± 60.7
TIM	8.38 ± 75.0	-15.26 ± 137.42	7.28 ± 88.01	-11.5 ± 80.41
TS	-7.22 ± 44.36	-28.83 ± 108.92	9.36 ± 62.53	12.25 ± 48.3
ETM	0.68 ± 45.56	15.69 ± 105.45	-1.51 ± 54.41	6.23 ± 41.72
QS	-0.95 ± 91.15	20.7 ± 174.27	-14.01 ± 109.35	7.78 ± 95.13
EKS	-12.37 ± 81.77	-1.46 ± 124.94	7.59 ± 79.41	-3.76 ± 79.68
AS	27.49 ± 110.15	-67.67 ± 149.13	34.51 ± 95.26	-52.98 ± 95.51
ETS	-28.83 ± 133.6	39.52 ± 254.97	-17.95 ± 153.68	-9.46 ± 114.21
CTS	-37.29 ± 119.41	-9.53 ± 212.26	20.92 ± 108.07	-15.67 ± 94.55
EP	-4.48 ± 81.05	-48.81 ± 128.24	1.52 ± 76.61	19.32 ± 121.28

References

Barandun M, Fiddes J, Scherler M, Mathys T, Saks T, Petrakov D and Hoelzle M 2020 The state and future of the cryosphere in Central Asia *Water Security* **11** 100072

Barandun M and Pohl E 2023 Central Asia's spatiotemporal glacier response ambiguity due to data inconsistencies and regional simplifications *The Cryosphere* **17** 1343–71

Yao T, Thompson L, Yang W, Yu W, Gao Y, Guo X, Yang X, Duan K, Zhao H, Xu B, Pu J, Lu A, Xiang Y, Kattel D B and Joswiak D 2012 Different glacier status with atmospheric circulations in Tibetan Plateau and surroundings *Nature Clim Change* **2** 663–7